FIBER OPTIC TEMPERATURE SENSORS USING LIGHT EMITTING DEVICES

A Thesis Submitted
in Partial Fulfilment of the Requirements
for the Degree of
MASTER OF TECHNOLOGY

by

URIMINDI NARASIMHULU

to the

DEPARTMENT OF LASER TECHNOLOGY
INDIAN INSTITUTE OF TECHNOLOGY KANPUR

APRIL 1990

LT-1990-M-NAR-F

CERTIFICATE

It is certified that the work contained in the thesis entitled "Fiber Optic Temperature Sensors using Light Emitting Devices" by "Urimindi Narasimhulu" has been carried out under my supervision and that this work has not been submitted elsewhere for a degree.

Dr. R. SHARAN

Department of Electrical Engineering

IIT KANPUR

April, 1990

ACKNOWLEDGEMENTS

When I think of my toils over the thesis, I feel that without the much needed guidance and encouragement of Dr. R. Sharan, it would not have been possible for me to complete this work. To work with him has been a lesson in sincerity, dedication and logical thinking. It is, therfore, with a deep sense of gratitude that I acknowledge my gratefulness to him.

I am extremely thankful to Dr. K. K. Sharma, Dr. P. K. Chatterjee and Dr. R. K. Thareja and all of my respected teachers who taught and helped me with their utmost and sincere efforts.

I really do not have words to thank Mr. Sandeep Agarwal and Mr Divakar of Physics dept. Their contribution to my work is respectfully acknowledged. I thank Dr. J. Narain, Mr. Ravindra kumar, and Mr. Abhay kumar for their kind help during my experiments. I take this opportunity to thank my colleagues Lalit, Rajnish, Brighu Sandeep kumar, Murali, Kasi, Hariprasad, Kanmani, Anando, Avinash Karandikar, Gattani, Subba Rao and Somany... who made my stay at IIT Kanpur a memorable one.

I will always remember my happy days in SBRA staying with my near and dear friends specially Ramesh, Srinivas, Nagarjun, Sarkar Venugopal, Nigam and Somany...

I am highly indebted to Sri. S. V. Ramanaiah, my school teacher, who is instrumental in cherishing my desire to learn. Finally I thank my wife Latha for her encouragement althrough the duration of this work.

U. Narasimhulu

April 24, 1990 (U. NARASIMHULU)

ABSTRACT

Name of Student: Urimindi Narasimhulu. Roll No: 8811609

Degree for which submitted: M.Tech. Department: Laser Technology.

Thesis Title: Fiber optic temperature sensors using light emitting devices.

Name of thesis supervisor:

1. Dr. R. Sharan

Month and year of thesis submission: April, 1990.

In the present work the results which have been obtained to explore the possibility of using the light emitting devices as temperature sensors are reported. Experiments have been performed with light emitting diodes (LEDs) of different types in order to measure the electroluminescent spectra and thereby to identify the material from which the device is fabricated. Temperature aging of LEDs is carried out so as to find their suitability as temperature sensors. In order to use LEDs as temperature sensors, they should have large power output change with temperature. From the experimental results presented it was observed that GaP:Zn.O red LEDs seem to be suitable as temperature sensors. The temperature dependence of the threshold current of a semiconductor laser can be exploited for use as temperature sensors. A circuit for the measurement of the threshold current of a semiconductor laser is designed and the result can be compared with the threshold current of the same laser obtained from the derivative measurements of the current-voltage characteristics of double heterojunction (DH) injection lasers. The temperature dependence of the current transfer ratio (CTR) of an optoisolator can also be exploited for use as temperature sensors.

CONTENTS

CHAPTER 1

INTRODUCTION

Sensors constitute an important component of a measurement system.Recently there has been a growing interest in fiber optic sensors, mainly because of their immunity to electromagnetic interference (EMI).This growth of interest can be summarised from the perusal of Table-1 [1] which contains a partial list of optical fiber sensors that have been developed.In the present work we are interested in fiber optic temperature sensors, a partial list of which is given in Table-2.

Optical fiber sensors can be placed in two basic families: Intrinsic and Extrinsic.In intr insic sensors, the light is modulated as it passes through the optical fiber which itself acts as the sensing medium.In extrinsic sensors the light is modulated in a region external to the fiber, which acts only to guide the light to and from the sensing region.This categorization helps to focus on the variety of optical modulation schemes and on instrumentation difficulties to produce an error-free light signal.

Extrinsic sensors may be categorized according to the way the light is modulated.A light beam may be characterised by several parameters as follows,

(1)phase (2)intensity (3)wavelength (4)polarisation.Under suitable conditions a range of physical parameters may interact with the light signal to produce modulation effect in one or more of the above parameters, the extent of this modulation being

related to the magnitude of the physical effect.Table-3 [2] summarises the possible modulation schemes and detection techniques.Such interaction forms the basis of optical sensing, offering high sensitivity and accuracy as well as the advantages mentioned in Table-4.Combining optical sensing with fiber optic transmission provides the basis for a wide range of sensing devices which can be suitable for a multitude of applications such as industrial plant, process control, aerospace and defence.

In the present thesis the results which have been obtained to explore the possibility of using the light emitting devices as temperature sensors are reported.The temperature dependence of the characteristics of light emitting diodes (LEDs), semiconductor lasers, and optoisolators are described in chapter-2.Experiments have been performed with LEDs of different types in order to fulfill the following tasks.

(1).Measurement of electroluminescent spectra of LEDs.

(2).Identification of the LED made from a particular material.

(3).Temperature aging of LEDs so as to find its suitability as temperature sensors.

In order to use LEDs as temperature sensors,they should have large power output variation with temperature.From the experimental results presented in chapter-3 it was observed that GaP:Zn,O red LEDs seem to be suitable as temperature sensors.However, we can make them even more suitable, if we can eliminate some of the problems faced in the experiment, like coupling of power to the fiber and detection of emission from the LED.

The temperature dependence of the threshold current of a

semiconductor laser can be exploited for use as temperature sensors.A circuit for the measurement of the threshold current of a semiconductor laser is designed and the result can be compared with the threshold current of the same laser obtained from the derivative measurements of the current-voltage characteristics of double heterojunction (DH) injection lasers.Chapter-4 describes the reliability aspects of LEDs and lasers.A review of fiber optic temperature sensors and their market areas are briefly dealt in chapter-5.Finally the study of light emitting devices as temperature sensors is concluded in chapter-6.

TABLE-1

FIBER OPTIC SENSORS	
Sensor	Method/Application
Oil content monitoring, particle sizing	Forward angle scatter
Correlation flow metering Lase/fiber optic doppler	Time of flight and cross-correlation using light scatter Doppler mesurement using polarisation preserving fibers.
Photoelastic effect	Birefringent fringe intensity changes as a function of applied strain
Spectroscopy	Gas and liquid absorption in hazardous spaces(mines),combustion control, Time resolved techniques, Fluorescence.
Photoluminescence	Movement of photoluminescent peak with Temperature.
Semiconductor absorption,fluorescence,liquid crystals...etc.	Absorption edge variation with temperature.

TABLE-1 CONTD...

Sensor	Method/Application
Polarimeter/Polarisation properties	Current measurement.Low birefringence fiber for Faraday effect etc.Special high birefringence fibers are now being developed.
Distributed sensors (can include microbend model transfer effects)	Continuous interrogation of remote fiber lengths,security,temperature (use of optical time domain reflectometry (OTDR) and nonlinear effects)
Interferometric sensors	Measurement of temperature,pressure acceleration,magnetic field.
Liquid level sensors and refractometers	Liquid level measurement,turbidity monitoring,and optical fiber refractometer using attenuation of cladding modes
Optical fiber gyroscopes and resonators	Measurement of rotation rates

TABLE-2

FIBER OPTIC TEMPERATURE SENSORS

Basic principle	Temperature range	Material used	Ref.
Temperature dependence of fluorescence decay time.	20-150°C (±1°C)	Crystal alexandrite	[24]
	15-130°C (±1°C)	Nd:glass	[25]
	35-46°C (±.3°C)	Pink ruby $Cr^{3+}:Al_2O_3$	[34]
	30-200°C (±5°C)	$BaClF:Sm^{2+}$	[35]
Temperature dependence absorption change in semiconductors/ other materials	-55-125°C (.1°C)	Ga As	[20]
	-60-200°C (±.5°C)	Nd:glass	[21]
	25-300°C (±10%)	Nd^{3+} doped glass	[22]
	-10-300°C (±1°C)	GaAs/CdTe	[23]
	20-180°C (±.2°C)	GaAs/CdTe	[36]
	25-45°C (±.05°C)	Thermochromic solution	[37]
	20-180°C (±.2°C)	Silicon	[27]

TABLE-2 CONTD...

Basic principle	Temperature range	Material used	Ref.
same as above	77-150K ($\pm$.5K)	Eu^{3+} doped fluoride glass	[38]
Raman back scattering	-30-67°C	-----	[26]
Change in λ distribution of fluorescence	25-160°C ($\pm$.3°C)	Pink ruby $Cr^{3+}:Al_2O_3$	[19]
Change of polarisation with temperature	25-180°C	Quartz crystal	[29]
Change of no.of fringes with temperature	20-140°C	Fiber	[30]

TABLE 3 - OPTICAL MODULATION SCHEMES AND DETECTION TECHNIQUES

Type of information	Physical mechanism	Detection circultry	Main limitations	Typical examples
1. Phase	Interference between signal and reference fibres (Mach-Zehnder monomode system) or different propagation modes in multimode fibre	Fringe counting, or fractional phase-shift detection	- Laser noise and stability - Measurement of small phase shifts. - Elimination of unwanted spurious effects (other physical variables)	- Fiber gyroscope and hydrophone. - Multimode gauge for dynamic pressure/strain measurement.
2. Intensity	Modulation of transmitted light by absorption, emission or refractive index changes	Analog (or digital for go/no-go transducers)	Normalisation for source intensity variations and, variable line and connector losses (at long distances)	- Strain/pressure gauge using modulated microbending loss. - Optical encoders.
3. Wavelength	Spectral-dependant variations of absorption emission and refractive index	Amplitude comparison at two fixed wavelengths, or analogue signal for scanned wavelength	Suitable scanned-wavelength sources. Wavelength dependant line loss	Temperature measurement by : - Variable Fabry-Perot cavity. - Birefringent crystal. - Semiconductor band gap shift.
4. Polarisation	Changes in the gyratory optical tensor	Polarization analyzer and amplitude comparison	Spontaneous (stress-induced) and inherent birefringence of fibers	Faraday-rotator magnetic-field transducer for current measurement of high-voltage transmission lines

TABLE-4

GENERAL ADVANTAGES OF OPTICAL FIBER SENSORS
(1).Safety, no spark risk.
(2).Low weight i.e. Useful for aerospace,oil plotforms.
(3).Immunity to interference, can be inserted near HV cables,transformers..etc.
(4).Do not emit RF.
(5).Low thermal mass, fast response for temperature measurement.Can be used to provide integrated measurement.
(6).Small size for medical applications, small volume investigations.
(7).Highly sensitive surface properties for throw-away medical sensors.
(8).Geometrical versatality for hydrophone windings,gradient magnetometers, extended hydrophones.
(9).Radiation sensitive for nuclear applications.
(10).Compatible with high bandwidth communications medium.
(11).Efficient carrier of power.

CHAPTER 2

TEMPERATURE DEPENDENCE OF THE CHARACTERISTICS OF LIGHT EMITTING DEVICES:

2.0.0. INTRODUCTION:

The present work is concerned with designing temperature sensors based on the temperature dependence of the characteristics of light emitting devices. Hence this aspect is described in the present chapter.

2.1.0. LIGHT EMITTING DIODES (LEDs):

Probably the main impetus which has stimulated work on the development of the LED is the high conversion efficiencies which have been obtained from GaAs p-n junctions. As early as 1965, a power efficiency of 40% had been achieved at low temperature with a hemispherical-shaped junction, As a result a considerable effort has been made into improving the room temperature efficiency of GaAs and in particular other materials with wider bandgaps which achieve efficient electroluminescence in the visible spectrum. The physical parameters of LEDs, as in all semiconductor devices, exhibit a dependence on temperature. The forward voltage/current relationship, quantum efficiency, and emitted wavelength are the temperature variant parameters of greatest interest to the LED user. The effect of temperature on each of the above parameters is considered in the following sections.

2.1.1. VARIATION OF FORWARD VOLTAGE WITH TEMPERATURE:

The forward voltage/forward current relationship for an LED can be expressed as

$$I_f = I_o \exp(qV_f/nkT)$$

where n is a function of temperature, I_f, and the nature of the recombination mechanism. Empirical results for both direct and indirect gap LEDs exhibit temperature coefficients of $-1.1mV/^{\circ}C$ to $-2.5mV/^{\circ}C$ depending on the forward current. Fig.2.1.0 depicts this relationship.

Fig.2.1.1 shows the V-T characteristics of the LED chip and provides a comparision with the commercial GaAs sensor. The V-T curve is nearly linear over most of the temperature range. Through a careful selection it is possible to pick a diode that exhibits better sensitivity at low temperatures if one is interested in using them as temperature sensors.[2].

2.1.2. VARIATION OF PEAK WAVELENGTH WITH TEMPERATURE:

The effective energy gap in both direct and indirect gap semiconductors tends to become slightly smaller with increasing temperature. This will result in slight increases in the emitted wavelength. For direct gap emitters the wavelength will increase by $0.2nm/^{\circ}C$. The wavelength of Nitrogen doped indirect gap emitters shows a somewhat lower dependency with typical positive variations of about $0.09nm/^{\circ}C$. Fig.2.1.2 shows the variation of wavelength temperature for GaP:N LEDs.[3].

2.1.3. VARIATION OF OUTPUT POWER WITH TEMPERATURE:

An increase in temperature generally decreases [4] the power output of luminescent diodes. This effect was due to an increase in internal absorption with increasing temperature. Using the radiative band pinch techniques to minimize internal absorption effects, it was concluded that the effect was due to a decrease in the internal quantum efficiency for radiative recombination with increasing temperature. Since a change in temperature induced

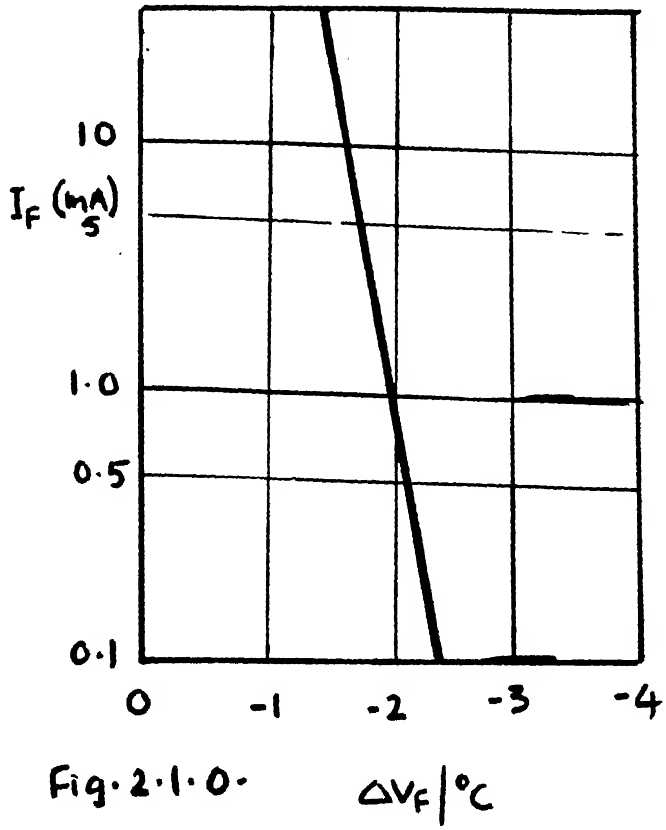

Fig. 2·1·0·

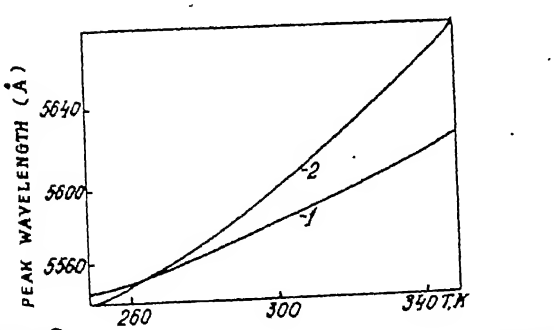

2·1·2
Temperature dependences of emission maximum spectral position for $Ga_{0.99}Al_{0.01}P$ (1) and GaP : N (2) LED's.

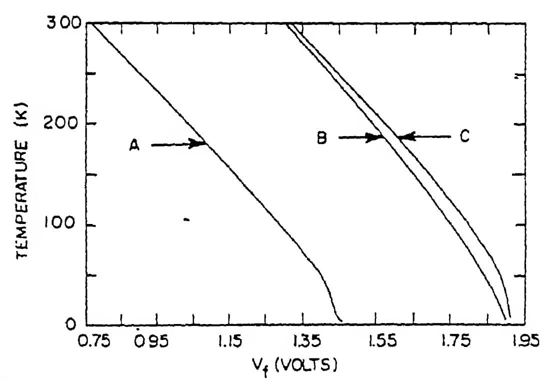

FIG. 2·1·1 Variation with temperature of the forward voltage V_f 10 μA. (A) Commercial GaAs diode sensor. (B) Monsanto re LED. (C) Radio Shack red LED.

Fig. 2·1·2

Fig. 2·1·1

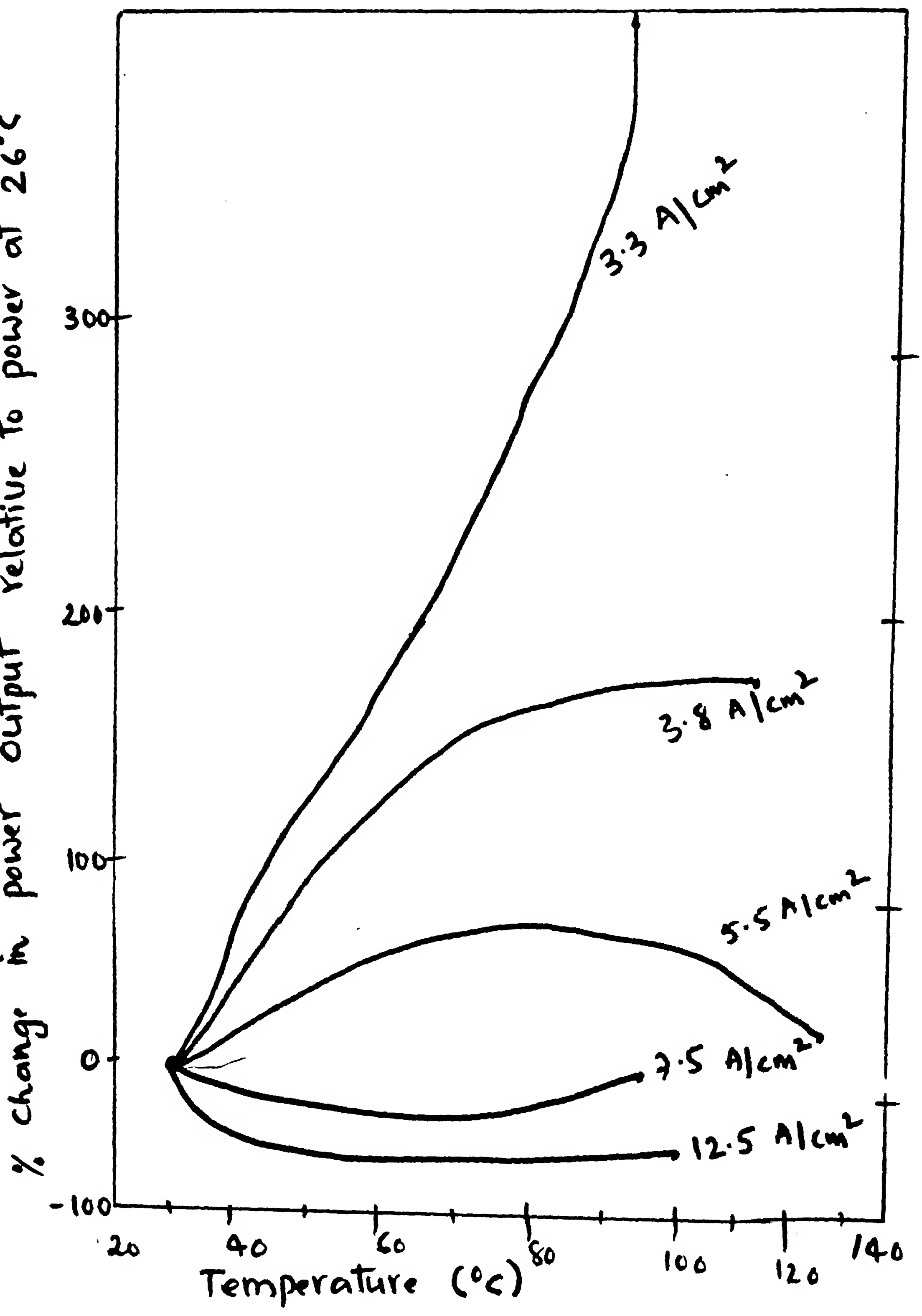

% change in power output relative to power at 26°C
300
200
100
0
-100
3.3 A/cm²
3.8 A/cm²
5.5 A/cm²
7.5 A/cm²
12.5 A/cm²
20
40
60
80
100
120
140
Temperature (°c)

Fig 2.1.3

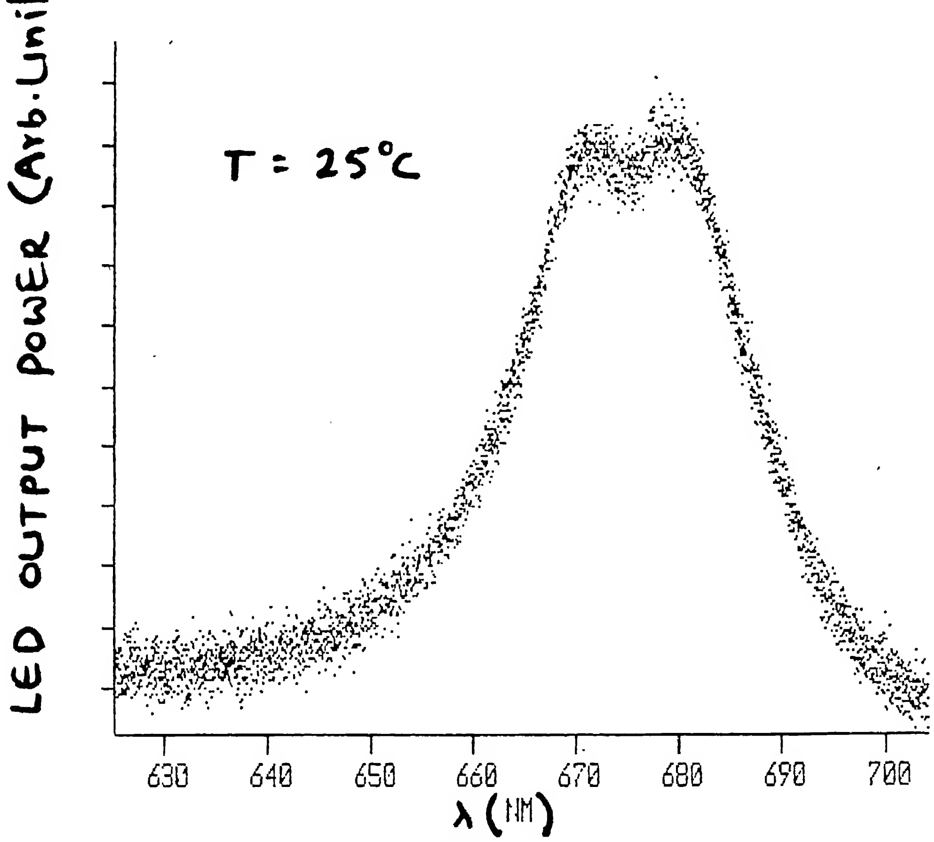

(a)

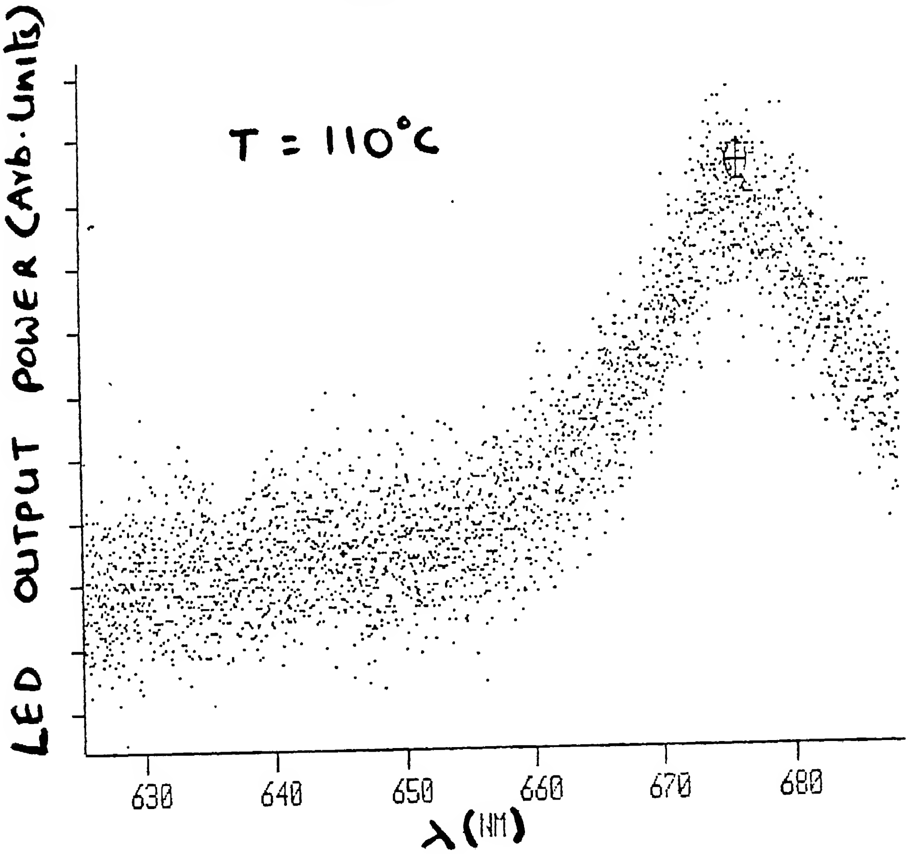

(b)

Fig 2.1.4 : Variation of LED output power with Temperature.

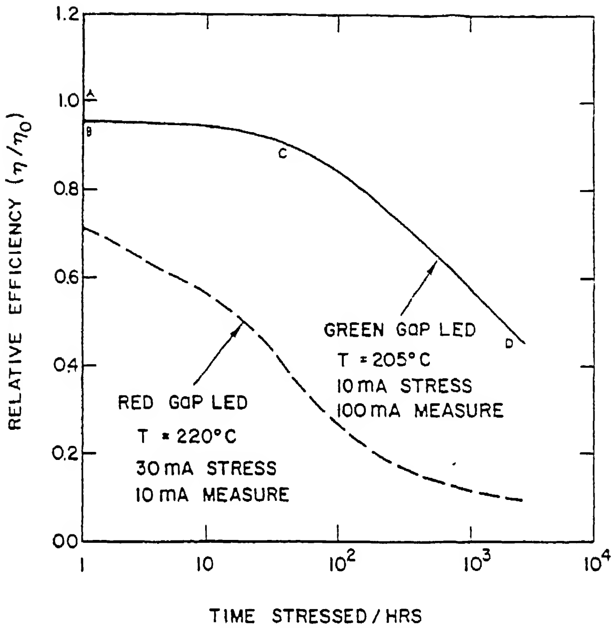

FIG.2.1.5 Degradation of relative electroluminescent efficiency (η/η_0) for green-light-emitting GaP LED's. Efficiency measurements are made at 100 mA (pulsed) and reflect directly the bulk radiative recombination efficiency. The dashed line represents the degradation of typical red-emitting GaP material, shown here for the sake of comparison.

Fig. 2.1.5

changes in the current and voltage across the device, it is necessary to carry out two sets of experimentsso as to obtain data with constant current and constant power output, the latter providing direct information on the temperature dependence of the radiative power efficiency of the diode.The results obtained at constant currents are shown in fig.2.1.3.The variation of the radiant power of an LED with temperature is of an order of -1%/°C and is typical for both direct and indirect gap materials.The change in luminous intensity of an LED exhibits a logarithmic relationship over large changes in temperature.Calculation of expected changes should be done using the following relationship:

$$L_{T1}=L_{TO}\exp(k\Delta T)$$

$$\Delta T=T_{O}-T_{1}$$

$$k=\ln(1-\text{temp.coefficient})$$

2.1.3. MEASUREMENT OF EMISSION SPECTRUM OF LED:

The electroluminescent spectrum of the LED is measured at room temperatureand is shown in fig.2.1.4a.Now the experiment is repeated at elevated temperatures of the order of 110°C.It is observed that the output spectrum decreases in amplitude and is shown in fig.2.1.4b.

2.1.4: TEMPERATURE DEPENDENCE OF THE DEGRADATION OF LEDs:

The dependence of LED emission on temperature can be attributed to several mechanisms,eg.bandgap dependence,variation of radiative and nonradiative mechanisms,changes in the injection efficiency at the p-n junction.Even over the limited temperature range of -40 to +100°C, there is no single dominant mechanism which can explain the observed characteristics.

In our effort to use LEDs as temperature sensors, the temperature dependence of the output power of these are

measured. Commercially available GaP:N, GaP:Zn,O, $Ga_{.7}Al_{.3}As$, $GaAs_{.6}P_{.4}$ LEDs are considered. All of the above LEDs can be classified colourwise as green and red. Let us discuss the degradation mechanism in each of these two types.

2.1.5. GREEN LEDs:

LEDs with light emission in the green part of the visible spectrum are commonly fabricated through liquid phase epitaxy (LPE) or vapour phase epitaxy (VPE) from the binary alloy GaP:N, where the isoelectronic trap nitrogen acts as an efficient radiative recombination center. Since the light output of such LEDs tends to degrade under normal operating conditions much effort has been put in reliability investigations to understand and identify specific degradation mechanisms.

In GaP:N LEDs of VPE material degradation is associated with a decrease in minority-carrier lifetime in the p-doped region of the diodes. This process can be described with a model assuming the generation of nonradiative recombination centers (NRC). In diodes of LPE material generation of NRCs are due to the formation of dislocations in the vicinity of p-n junction and these can be found by using transmission electron microscopy (TEM). On the other hand the variation in the light output of GaP:N LEDs of VPE material might also be related to the displacement of nitrogen atoms eventually associated with the creation of NRCs.**[5]**.

Green LEDs exhibit a degradation of quantum efficiency which becomes important, under relatively severe stress aging conditions. A representative example of the degradation behaviour of these devices under temperature stress-aging conditions

($T \leq 205^{\circ}C$) is shown in fig.2.1.5.[6].Here the normalized efficiency η/η_o is plotted as a function of time.The TEM observation at this temperature shows that the slow bulk electroluminescence degradation may be accounted for by the formation of new dislocations in the vicinity of the p-n junction plane.These dislocations develop a climb process in the p-n junction vicinity from the original dislocations in the epitaxial layers.The climb process may be promoted by an enhanced mobility of interstitial defects due to nonradiative recombination of electron-hole pairs at the defect site.

Another investigation of green LED degradation [7] concludes that the migration of interstitial zinc towards and across the junction in devices prepared by liquid phase growth is responsible for the slow degradation of the emission.

2.1.6. RED LEDs:

Degradation of bulk radiative recombination efficiency plays a dominant role in the degradation of GaP red LED quantum efficiency, which is aged at elevated temperatures,[8]. Apart from this major degradation mechanism, there are two more failure mechanisms and both caused a reduction of the ratio of the electron diffusion current $I_{\bullet}$ to total device currentI.Since only the electron diffusion component of the total diode current is effective in producing the electroluminescence, a reduction of $I_{\bullet}$ relative to I causes a degradation of device quantum efficiency.

The first of these failure mechanisms was a large increase in nondiffusion current components which were most apparent when the LED chip was bonded p-side up.This increase in nondiffusion

current tends to drop the injection efficiency of minority carriers and, consequently, the light output at a given total device current. In devices currently being fabricated which are also bonded p-up, this reduction in minority carrier injection efficiency not observed. The second failure mode was inferred in devices bonded p-side down which did not exhibit the large increase in nondiffusion current components shown by their p-up counterparts. In this case electroluminescence degradation was imputed to a reduction in minority carrier hole diffusion length on the n-side of the junction. At a given total diffusion current I_d this effect would reduce the electroluminescence efficiency by enhancing the minority hole injection into the n-side at the expense of the light producing minority electron diffusion current I_e.

There have been comments that, in red $GaAs_{.6}P_{.4}$ LEDs, zinc diffusion source type, arsenic overpressure and n-type dopant and concentration govern the internal quantum efficiency and the degradation rate of these devices,[9]. There have also been reports that native defects are generated during operation and these are responsible for degradation. This has a similarity with mechanisms suggested for GaAlAs DH lasers and GaAs high radiance LED degradation.

2.1.7. DEGRADATION ANALYSIS OF GaP:Zn,O LEDs:

In analysing the degradation of ZnO-doped GaP LEDs, it is useful to factor the external electroluminescent efficiency into several components:[10]

$$\eta(I) = \eta_B . f(I_e) . R . \eta_{inj}(I) . \eta_{oc} \qquad (2.1.0)$$

Here, I is the total device current, η_B is the bulk

electroluminescent efficiency at low injection levels, and $f(I_e)$ is the factor that accounts for saturation of ZnO centers at higher levels of electron diffusion current I_e.R is the ratio of electron diffusion current I_e to the total diffusion current, $I_e+I_h \cdot \eta_{inj}(I)$ is the ratio of total (hole and electron) diffusion current to the total device current I.Finally η_{oc} is the efficiency of extracting an electroluminescent photon from the LED chip and should be of the order of 50-60%.Although any of the factors in equation (2.1.0) can contribute to device degradation, the dominant loss will be shown to be from the $\eta_B \cdot f(I_e)$ product.The optical coupling efficiency η_{oc} is chiefly dependent on chip geometry, refractive index of the encapsulant, surface roughness, and contact absorbance.None of these shown to vary with degradation.The injection ratio R for abrupt p-n junction is given by

$$R = \left[1+ \frac{D_h}{D_e} \frac{N_A}{N_D} \frac{L_e}{L_h} \right]^{-1} \qquad (2.1.1)$$

where D and L are the diffusion coefficients and diffusion lengths of minority carriers, and N_A and N_D are the net acceptor and donor concentrations,respectively.Capacitance measurements after degradation reveal no detectable changes in the doping densitiesN_A and N_D.If the minority diffusion coefficients (or their ratio) do not vary,the injection ratio soley depends on the ratio of minority diffusion length.

These diffusion lengths have been measured by scanning electron microscopy (SEM) for several well-characterized typical samples at 200°C.Based on the analysis of ~10 measurements before and after degradation at distances of ~2μm from the p-n junction,

the undegradaed diodes show average diffusion lengths $\langle L_{eo}\rangle$=.85μm and $\langle L_{ho}\rangle$=.36μm.The degraded values are $\langle L_{e}\rangle$=.42 and $\langle L_{h}\rangle$=.22μm. These values may be substituted in (2.1.1) to obtain the injection ratios before and after degradation, R_o.and R:

$$\frac{R}{R_o} = \left\{ \frac{1+D_h N_A L_{eo}}{D_e N_D L_{ho}} \right\} \left\{ \frac{1+D_h N_A L_e}{D_e N_D L_h} \right\}^{-1} \qquad (2.1.2)$$

$$= \frac{0.71}{0.67} = 1.07$$

Here the values of $N_D=1.1*10^{18}$ cm^{-3},$N_A=3.4*10^{17}$ cm^{-3}, $D_e=4.1$ cm^2/sec and $D_h=2.8$ cm^2/sec have been used and assumed unchanged with degradation.The electroluminescent efficiency of the same diodes had been reduced to η/η_o=0.1, measured at 10mA.Therefore the change in the injection ratio R, although appreciable,is not a major factor

At this point ,R and η_{oc} can be fairly eliminated as major factors in LED degradation.The remaining fatcors are η_B $f(I_e)$, the modulated bulk efficiency,and η_{inj}, the ratio of diffusion to total current.It is possible to measure the low level bulk efficiency variation directly by measuring the change in light output L at a fixed voltage bias chosen to be low enough that series resistance effects in the LED and saturation of ZnO centers is negligible.Under these conditions one has

$$L = \eta_B I_e = \left\{ \eta_B q \, (D_e)^{1/2} \, n_i^2/N_A \tau_e^{\,1/2} \right\} \exp\,(qV/kT) \qquad (2.1.3)$$

where n_i is the intrinsic carrier concentration and τ_e is the minority electron lifetime.It can be shown that at loe levels of electron injection the degradation of bulk efficiency η_B/η_{Bo}

equals the degradation of minority electron lifetime τ_e/τ_{eo}. One has then

$$\eta_B/\eta_{Bo}=\tau_e/\tau_{eo} \qquad (2.1.4a)$$

and

$$L/L_o= \eta_B I_e/\eta_{Bo} I_{eo}=(\tau_e/\tau_{eo})^{1/2}=(\eta_B/\eta_{Bo})^{1/2} \qquad (2.1.4b)$$

These L/L_o data are thus independent of excess current effects like space-charge recombination,surface leakage, and possible tunneling, as well as hole diffusion in to the n-side of the junction and allow a direct measure of the change in the bulk efficiency.It is noted that the so called "rapid" component of aging in these LEDs is a bulk recombination effect unrelated to surface contamination which may acrue gradually in the course of aging.

The remaining factor in Eq.2.1.0 is the ratio of diffusion to total diode current.This efficiency,like the injection ratio R,can actually be enhanced during bulk degradation.Qualitatively, this enhancement may be understood as follows:As a consequence of bulk degradation, the diffusion lengths of minority carriers are reduced, thus increasing the total diffusion current at a given level of bias voltage.For these diodes, where the rapid bulk degradation can occur, this effect can initially outstrip the increase in nondiffusion current components.

Even an approximate calculation of the injection efficiency is complicated in two respects:accounting for the voltage dependence of nondiffusion current components as the diodes degrade and measuring the initial diffusion current.In order to obtain a reasonable estimate of injection efficiency variation the following assumptions are made:

The voltage dependence of all nondiffusion current components through out degradation will be accounted for by an approximate space-charge current model:

$$I_{sc}(V)=I_{sc}^{o}\exp(qV/kT) \qquad (2.1.5)$$

The assumption that Eq.2.1.5 is valid through out degradation, will make the calculation of η_{inj} pessimistic as degradation proceeds.

The initial diffusion current is then taken to be the difference

$$I_{do}(V)= I_{o}(V)-I_{sco}(V) \qquad (2.1.6)$$

where $I_o(V)$ is the total initial measured current at V.Subscript o indicates the undegraded case.An estimate of the increase in total diffusion current requires the result obtained above that injection ratio R does not change significantly with degradation, i.e the increase in the hole injection proportional to the increase in electron injection.From (2.1.3)and(2.1.4a) it can be shown that

$$I_d/I_{do}=(\tau_{eo}/\tau_e)^{1/2} = L_o/L \qquad (2.1.7)$$

Injection efficiency may then be estimated from L-I-V data taken at various stages of degradation.Analysis has established the following points.

1).Degradation of this material is dominated by the reduction of the radiative recombination efficiency of minority carriers.

2).Other degradation modes have negligible influence over the useful operating life of the device.

SEMICONDUCTOR LASERS

2.2.0. INTRODUCTION:

One of the most important parameters of a semiconductor laser is its threshold current. Device structures and material properties have been optimized over the years, so that threshold currents are now low enough for most applications. During this period also the gradual increase in threshold current during device operation has been the overriding concern in trying to make a reliable device.

2.2.1. FACTORS DETERMINING THRESHOLD CURRENT:

The threshold condition of a semoconductor lasers can be expressed as the gain being equal to the total losses. This condition determines the threshold carrier density n_{th} since the material gain and loss depend on the carrier density. n_{th} and the carrier lifetime τ_s determine the threshold current I_{th}. Thus the temperature characteristics of I_{th} are determined by those of the gain, the loss, and the carrier lifetime. The intervalence band absorption is related to the loss and reduces the differential quantum efficiency η_d, while the nonradiative recombination (in particular, the Auger effect) and the carrier leakage over the heterobarrier determine the carrier lifetime. These relations are schematically shown in fig.2.2.1

The effects of the absorption loss, nonradiative recombination, and heat resistance of laser diodes on the temperature dependence of the threshold current of GaInAsP/InP lasers are derived by a systematic measurement of gain, loss, spontaneous emission efficiency, and carrier lifetime.

2.2.2. MEASUREMENT OF CARRIER LIFETIME AND SPONTANEOUS EMISSION EFFICIENCY:

The carrier density n can be connected with the injection I using the carrier lifetime τ_s,[11]

$$I = eVn/\tau_s . \tag{2.2.1}$$

τ_s can be written

$$1/\tau_s = 1/\tau_R + 1/\tau_{NR} \tag{2.2.2a}$$

$$= \bar{B}_R(n + p_o) + (\bar{A} + \bar{B}_{NR}n + \bar{C}n^2) \tag{2.2.2b}$$

$$= 1/(\tau_R \eta_{spon}) \tag{2.2.2c}$$

$$= B_{eff}n^{\gamma-1} \tag{2.2.2d}$$

where τ_R and τ_{NR} are the radiative and nonradiative recombination times, respectively. $1/\tau_R$ and $1/\tau_{NR}$ are expanded in to the power series of n as in the first and second brackets in (2.2.2b), repectively, where $\bar{B}_R$ is the radiative recombination coefficient and p_o is the acceptor concentration. $\bar{A}$, $\bar{B}_{NR}$ and $\bar{C}$ are the nonradiative recombination coefficients for which the nonradiative recombination centers, the carrier leakage, and the Auger effect are responsible, respectively. η_{spon} is the spontaneous emission efficiency defined as $(1 + \tau_R/\tau_{NR})^{-1}$. Eq. (2d) is the experimental formula for τ_s where the B_{eff} and γ are the constants with respect to n and temperature. Typical values of $B_{eff} = 1.5\text{-}2.0 \times 10^{-10}$ cm^3/sec and $\gamma \simeq 2$ for InGaAsP/InP lasers.

Radiative and nonradiative components of the carrier recombination can be estimated by the measurements of η_{spon} and τ_s. The measurements of η_{spon} and τ_s have been made for 1.58μm

wavelength surface emitting LEDs.This diode structure is similar to that of the laser considered in this discussion.

Fig.2.2.2 shows the spontaneous emission efficiency obtained from the pulsed current-light output characteristics as a function of temperature for different current densities.carrier lifetime τ_s was measured from the turn-on delay of the light output.From the results on τ_s and η_{spon}, τ_R and τ_{NR} in (2.2.2a) were obtained.Applying (2.2.2b) to τ_R and τ_{NR}, the coefficients $\bar{B}_R$ $\bar{A}$, $\bar{B}_{NR}$, and $\bar{C}$ were estimated.It was found that $\bar{A}$ small enough to be neglected at 150K<T< 400K, $\bar{C}$ = $4.0*10^{-29}$ cm^6/s being almost constant with respect to temperature, and that $\bar{B}_{NR}$ increased rapidly with temperature.The ratio $\bar{C}n^2/\bar{B}_{NR}n$, which roughly expresses the ratio of the Auger recombination to the carrier leakage, was 29%/71% in τ_{NR} at room temperature with $n=1.0*10^{18}$ cm^{-3}.All of these contributions determine the carrier density dependence of the total carrier lifetime τ_s, according to (2.2.2b) and this is shown in fig.2.2.3 together with experimental data for τ_s, τ_R and τ_{NR} at T=294K and 154K.And from (2.2.2) the threshold current I_{th} is written as

$$I_{th}=eVn_{th}/(\tau_R\eta_{spon}) \qquad (2.2.3a)$$

$$\simeq eVB_{eff}n_{th}^{\gamma} \qquad (2.2.3b)$$

where n_{th} is the threshold carrier density.

2.2.3. MEASUREMENT OF LOSS BY DIFFERENTIAL QUANTUM EFFICIENCY:

The loss coefficient in the laser cavity, α_{loss}, can be related to the differential quantum efficiency η_d as

$$\eta_d = \eta_{stim}\ \ln(1/R)/[\alpha_{loss}L + \ln(1/R)] \qquad (2.2.4)$$

where L is the cavity length, R is the reflectivity of the end mirrors, and η_{stim} is the internal efficiency of stimulated

emission, which should be defined separately from that of η_{spon}. η_{stim} can be approximated unity, since the rates of the nonradiative recombination and carrier leakage are much smaller than that of the stimulated laser transition above threshold.The α_{loss} can be written as

$$\alpha_{loss} = \xi\alpha_{ac} + (1-\xi)\alpha_{ex} \tag{2.2.5}$$

where ξ is the optical confinement factor, α_{ac} and α_{ex} are the loss coefficients in the active region and the cladding region respectively.α_{ac} is mainly due to the intervalence band absorption which can be written as

$$\alpha_{ac} = \alpha_1 + \alpha_2$$

$$= K_o n + \alpha_2 \tag{2.2.6}$$

where α_1 is the loss coefficient due to the transitions between the split-off and heavy-hole valence band, K_o is the constant proportionalitiy connecting the carrier density n with α_1,and α_2 is the loss coefficient due to the transition between the split-off band and the acceptor level, which is almost constant for n.

The effective stripe width of the laser whose η_d was measured was obtained to be 26μm from the half power width of the near field pattern below threshold.Measurements were made under cw and pulsed (500 nswidth, 1kHz repetition) condition,and the output power was measured using Ge photodiode whose sensitivity was carefully calibrated in order to take into account the wavelength variation of the laser due to temperature.Measured results are shown in fig.2.2.4.As can be seen η_d decreases rapidly with temperature above about 250K.

The loss coefficient in the active region α_{ac} was obtained from measured η_d (pulsed) as shown in fig.2.2.4 using (2.2.4) and (2.2.5).The value of α_{ex} in (2.2.5) is estimated to be 5.6 cm^{-1} at T=300K and the values of ξ and R in (2.2.4) and (2.2.5) are as ξ=0.5 and R=.42 respectively.The measured results of the absorption loss are shown in fig.2.2.5.

As can be seen in fig.2.2.5, α_{ac} increases with temperature, where as η_d decreases.The dashed curves are calculated α_1 and α_2 values from (2.2.6), and the solid curve is calculated $\alpha_1+\alpha_2$, respectively.The temperature dependence of the measured α_{ac} is in good agreement with theoretical solid curve.

2.2.4A. GAIN MEASUREMENT:

The net gain including losses is obtained by the ratio between the top and bottom of the spectra of the amplified spontaneous emission.Here we wish to discuss the temperature characteristics of the gain as a function of the carrier density rather than the injection current, so as to eliminate the effects of the nonradiative recombination and the carrier leakage.Carrier density is obtained applying (2.2.1) and (2.2.2) to the injection current.The peak values of the measured netgain coefficient as a function of carrier density for different temperatures are shown in fig.2.2.6.The gain in this figure includes the mirror loss,i.e gain=0 at threshold.As can be seen,the peack values of the net gain can be related linearly with the carrier density n.

2.2.4B. FORMULATION:

The results obtained in fig.2.2.6 can be formulated as follows.The peak value of the netgain coefficient(including losses) g_p can be expressed as

$$g_p = \xi A_o(n-n_g)-[\alpha_{loss}+\ln(1/R)/L\ ]$$

$$= \xi(A_o n-\alpha_{in})-[\alpha_{loss}+\ln(1/R)/L\ ] \qquad (2.2.7)$$

where the terms in the brackets express the material gain,i.e,the gain due to the electron-hole pairs, A_o is a constant, n_g is the carrier density at which the material gain changes from negative to positive, and α_{in} is equal to $A_o n_g$.

Using (2.2.5) and (2.2.6), the peak value of the netgain coefficient g_p in (2.2.7) is written

$$g_p= \xi(A_o-K_o)n-[\xi(\alpha_{in}+\alpha_2)+(1-\xi)\alpha_{ex}+\ln 1/R)/L] \qquad (2.2.8)$$

The carrier density dependence of the netgain is arising not only fromthe material gain ($A_o n$) but also from the loss due to the intervalence band absorption ($K_o n$).

The gradient of the curves in fig.2.2.6 are corresponding to $\xi(A_o-K_o)$ in (2.2.8).The temperature dependence of the values of (A_o-K_o) obtained from fig.2.2.6 are shown in fig.2.2.7.(A_o-K_o) obtained are decreasing rapidly with increasing temperature above about 250K.This is due to intervalence band absorption.From the best fitting (fig.2.2.6), (A_o-K_o) can be determined experimentally as $4.4*10^{-15}\exp(-T/85)$ cm^2 above 250K.

From the results of the gain and loss obtained above, the threshold carrier density n_{th} can be determined by the threshold condition g_p=0.From (2.2.4)-(2.2.8) this condition gives

$$n_{th}=[\alpha_{in}+\ln(1/R)/(\xi\eta_d L)]/A_o \qquad (2.2.9a$$

$$=[(\alpha_{in}+\alpha_2)+\alpha_{ex}(1-\xi)/\xi+\ln(1/R)/L]/(A_o-K_o) \qquad (2.2.9b)$$

The influence of the intervalence band absorption is includedin n_{th} through η_d in (2.2.9a) or K_o in (2.2.9b).

2.2.5. TEMPERATURE DEPENDENCE OF THRESHOLD CURRENT:

A: Effects of intervalence band absorption, nonradiative recombination, and carrier leakage:

All the parameters required for the analysis of the threshold current I_{th} have been obtained experimentally as mentioned above. We can now discuss howmuch the absorption and the nonradiative components contribute to the temperature dependence of the threshold current I_{th}.

The temperature dependence of I_{th} obtained from (2.2.3) and (2.2.9) are shown in fig.2.2.8. The dashed curve in this figure is given by excluding the effects of the intervalence band absorption and the nonradiative component, namely $\eta_d=1$ and $\eta_{spon}=1$ in (2.2.9a) and (2.2.3b), where I_{th} decreases with temperature. In this case, the temperature dependence of I_{th} is due to those of the n_{th} and the radiative recombination (as expressed in (2.2.3a)). The gain decreases with temperature as seen in figs.2.2.5 and 2.2.6 due to the spreading of the carrier distribution in the energy bands, and, therefore, the threshold carrier density n_{th} increases with temperature. The radiative recombination time τ_R also increases with temperature as seen in fig.2.2.3. The decrease of the dashed cureve in fig.2.2.6 implies that the τ_R increases more rapidly than the n_{th}.

The dot-dashed line in fig.2.2.6 is obtained by excluding only the effect of the intervalence band absorption, namely $\eta_d=1$, where the I_{th} increases with the exponential temperature coefficient of T_o=145K. The solid curve in fig.2.2.6 is obtained by including the effects of both the absorption loss and the nonradiative component where I_{th} increases with T_o=60K at room temperature. Both effects significantly contribute to the

temperature characteristics.The change of T_o=145K to T_o=60K is due to the effect of intervalence band absorption

B: Heating effect:

For continuous operation it is necessary to take in to account heating effects due to the injection current.The temperature increase ΔT at the cw threshold current $I_{th}^{cw}(T)$ is given by

$$\Delta T = I_{th}^{(cw)^2}(T) r_d R_H + I_{th}^{cw}(T)(1-\eta_{spon}) V_D R_H \qquad (2.2.10)$$

where the first term in the right-hand side is due to the Joule heating, where r_d and R_H are the series resistane and the heat resistance, respectively, and the second term is due to the nonradiative recombination, where V_D is the applied junction voltage of the laser, which is nearly equal to the band gap energy in electron volts.Here the heating due to the optical absorption losses is neglected,since the radiation in the active region is small at the threshold.$I_{th}^{cw}(T)$ can be related to the pulsed threshold current $I_{th}(T)$ of (2.2.3) by

$$I_{th}^{cw}(T) = I_{th}(T+\Delta T) \qquad (2.2.11)$$

Thus $I_{th}^{cw}(T)$ can be calculated by combining (2.2.10) and (2.2.11).

The η_d near the threshold measured under continuous operation $\eta_d^{cw}(T)$ can be given

$$\eta_d^{cw}(T) = \frac{\partial}{\partial I}\left[\eta_d(T+\Delta T)\left\{I - T_{th}(T+\Delta T_1)\right\}\right] \cdot \left[\frac{I + I_{th}^{cw}(T)}{\Delta T_1 + \Delta T}\right]$$

$$= \eta_d(T+\Delta T) \cdot \left[\frac{1 - 2 I_{th}^{(cw)^2}(T)\; r_d R_H}{T_o - \Delta T + I_{th}^{(cw)^2}(T)\; r_d R_H}\right] \qquad (2.2.12)$$

where ΔT_1 is the temperature rise due to the current I_1 which is

given by

$$\Delta T_1 = I^2 r_d R_H + I_{th}^{cw}(T+\Delta T_1)(1-\eta_{spon})V_D R_H,$$

and the characteristic temperature T_o is defined by

$$T_o = I_{th}^{cw}/(\partial I_{th}^{cw}/\partial T). \qquad (2.2.13)$$

The maximum temperature for cw operation, T_{max} is obtained from the condition $(\eta_d^{cw}(T_{max})=0$ in (2.2.12), which gives $\Delta T = T_o + I_{th}^{(cw)^2}(T_{max}) r_d R_H$. I_{th}^{cw} and η_d^{cw} using (2.2.1)-(2.2.12) with identical measured parameters are shown in fig.2.2.9., compared with the measured results on the buried heterostructure (BH) lasers A emitting at 1.62μm and B at 1.5μm wavelength.The values of r_d and R_H were assumed to be 10Ω and 100°C/W for the former, and 10Ω and 50°C/W for the latter respectively.The sample B in fig.2.2.9 show higher temperature operation with higher η_d.This is because the active layer is thin, thus ξ is small (ξ=0.18 for sample B while it is 0.64 for A) which reduces the effective absorption.

Calculations agree well with the measured results, where th heating effect enhances the intrinsic temperature dependence of I_{th} and η_d (in particular that due to the intervalence band absorption) at the maximum operating temperature.The maximum cw operation temperature differs for each laser .This is because T_{max} depends on r_d, R_H and I_{th} in addition to the intrinsic temperature characteristics.Fig.2.2.10 shows the calculated maximum cw operation temperature T_{max}(°C) as a function of the I_{th}(pulsed) at 300K for different values of heat resistance with the assumption of the series resistance r_d=5Ω, and the junction voltage V_D=0.75V

As can be seen from fig.2.2.10, T_{max} depends strongly on I_{th}

which can be reduced by optimizing the structure parameters, such as the volume of the active region, the light confinement factor. For example to make T_{max} larger than 150°C requires the condition of I_{th} smaller than 15mA, r_d is smaller than 5Ω and R_H is smaller than 20°C/W.

Fig.2.2.11 shows the calculated η_d and threshold current density (pulsed) of a 1.6μm wavelength laser as a function of optical confinement factor ξ. η_d higher than 50% is expected for ξ of smaller than .1 at ln(1/R)/L=30 cm^{-1}.

2.2.6. GENERAL EXPRESSION FOR THRESHOLD CURRENT:

General expression for the threshold current as a function of temperature can be obtained by solving (2.2.13) and is given by $I_{th} = I_o \exp(T/T_o)$ where I_o is a constant and T_o is characteristic temperature often used to express the temperature sensitivity of threshold current. For AlGaAs lasers the observed $T_o \geq 120K$ near room temperature, while for InGaAsP lasers the I_{th} increases more rapidly with increasing temperature. The high temperatutre sensitivity of the I_{th} of InGaAsP lasers limits their performance under high temperature operation. Furthermore, under cw operation at room temperature the maximum power emitted by these lasers is limited by as thermal runaway process: more and more current is required to offset the effect of the internal temperature increase and this inturn further increases the temperature.

2.2.7. CONCLUSION:

The effects of the absorption loss and the nonradiative current component on the temperature dependence of the threshold current of InGaAsP/InP lasers for 1.5-1.6 μm wavelength range are

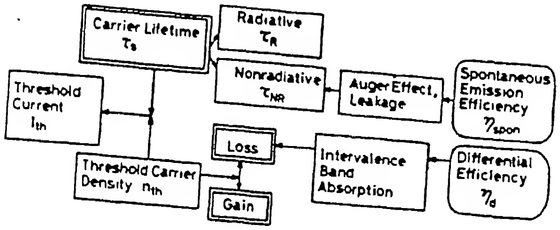

fig.2.2.1

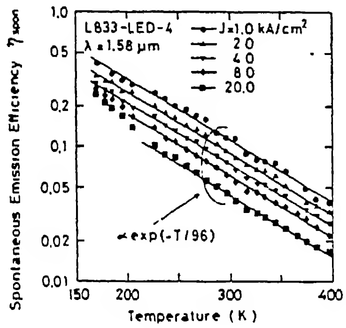

Fig 2.2.2

The temperature dependence of the spontaneous emission efficiency η_{spon} measured on a 1.58 μm wavelength surface emitting LED for different current densities [12]. Emitting diameter and active layer thickness of the LED are 50 μm and 0.26 μm, respectively.

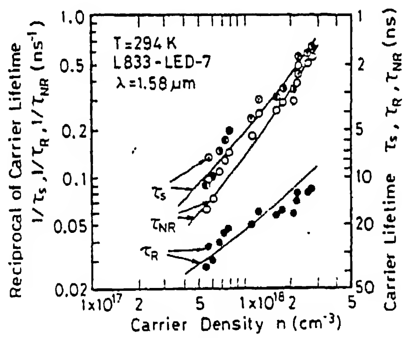

(a)

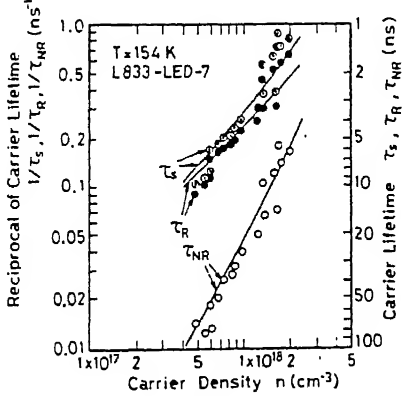

(b)

Fig 2.2.3

The reciprocal of the carrier lifetime $1/\tau_s$, the radiative and nonradiative recombination times ($1/\tau_R$ and $1/\tau_{NR}$) as a function of carrier density n obtained for a 1.58 μm wavelength surface emitting LED at (a) $T = 294$ K and (b) $T = 154$ K. The expressions of (2b), i.e., series expansion for n, are fitted to the measured results in order to obtain the recombination coefficients in (2b) (solid curves).

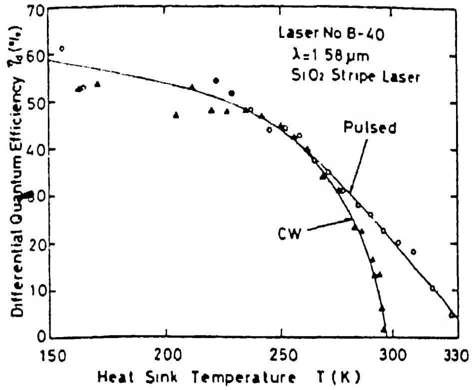

← fig 2.2.4

The temperature dependence of the differential quantum efficiency η_d measured on a 1.58 μm wavelength GaInAsP/InP SiO_2 stripe laser. The volume of the active region is 360 μm (length) × 18 μm (stripe width) × 0.2 μm (thickness).

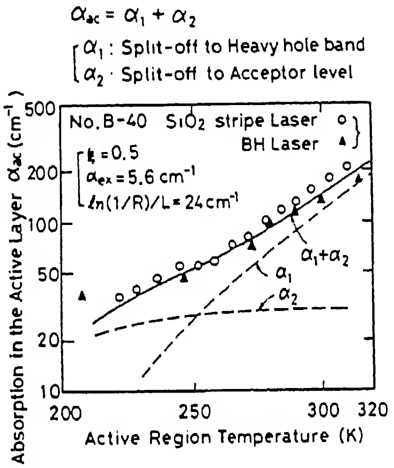

← fig 2.2.5

. The loss coefficient in the active region α_{ac} obtained from Fig. 4. The dashed curves are the theoretical calculations of the intervalence band absorption [redacted] (transitions between heavy-hole and split-off bands α_1 and split-off band to acceptor level α_2), and the solid curve is $\alpha_1 + \alpha_2$.

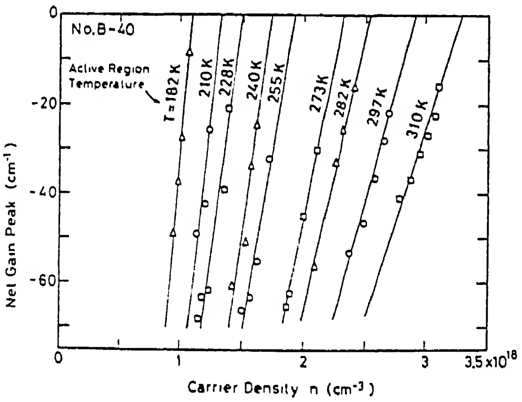

The peak value of the net gain coefficient of the 1.58 μm wavelength GaInAsP/InP SiO_2 stripe laser as a function of the carrier density for different temperatures. The gain in the figure includes the mirror loss, i.e., the threshold is at gain = 0. A linear relation can be applied between the net gain coefficient and the carrier density.

↑

2.2.6 – fig 2.2.7 ⟶

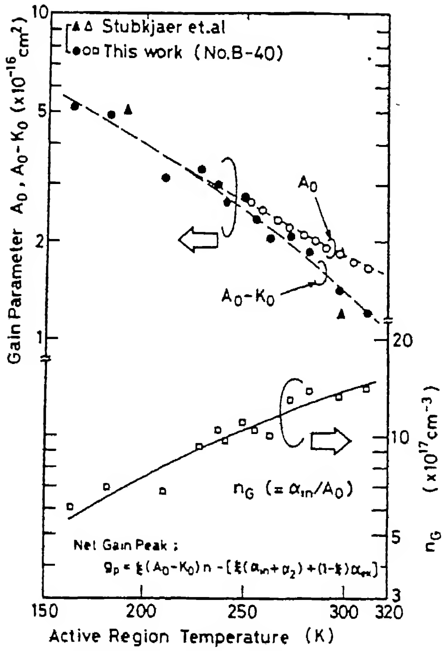

The temperature dependence of the gain parameters in (8) obtained from Figs. 5 and 6, where A_0 is the proportionality constant of the material gain to the carrier density n, K_0 is that of the intervalence band absorption, and n_G is the carrier density at which the material gain changes from negative to positive.

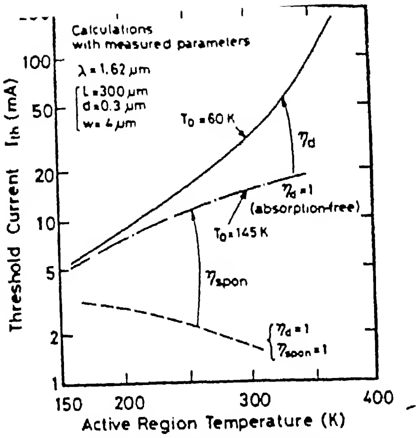

The temperature dependence of the threshold current I_{th} calculated using the measured results of the gain, the loss, and the carrier lifetime. The volume of the active region is assumed to be 300 μm (length) × 4 μm (width) × 0.3 μm (thickness). The calculations were made for the three cases: 1) the intervalence band absorption and nonradiative components are included (solid curve), 2) $\eta_d = 1$, i.e., absorption-free (dot-dashed curve), 3) both $\eta_d = 1$ and $\eta_{spon} = 1$ (dashed curve).

↑
fig 2.2.8

fig → 2.2.9

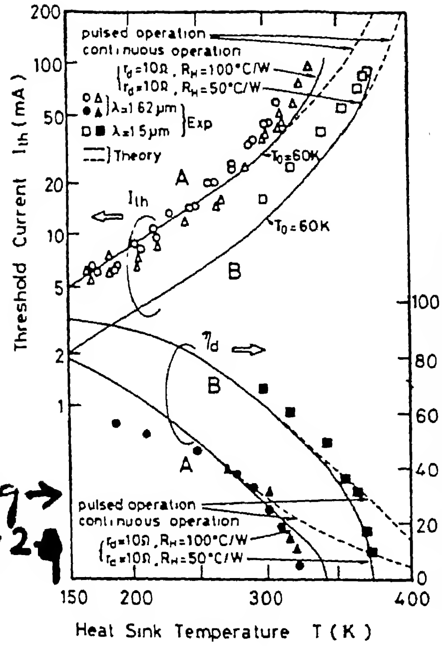

The threshold current I_{th} and the differential quantum efficiency η_d calculated for continuous operation, compared with the results measured on buried heterostructure lasers with different volumes of the active region (A[redacted] and B[redacted] in the figure). The volumes of the active region are 300 μm (length) × 4 μm (width) × 0.3 μm (thickness) for A and 200 μm × 1 μm × 0.1 μm for B.

fig 2.2.10 →

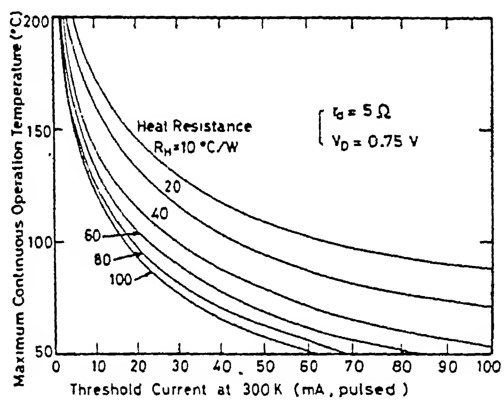

Maximum CW operation temperature T_{max} (at which $\eta_d^{(CW)} = 0$) as a function of pulsed threshold current at 300 K for different values of heat resistance R_H.

fig 2.2.11 →

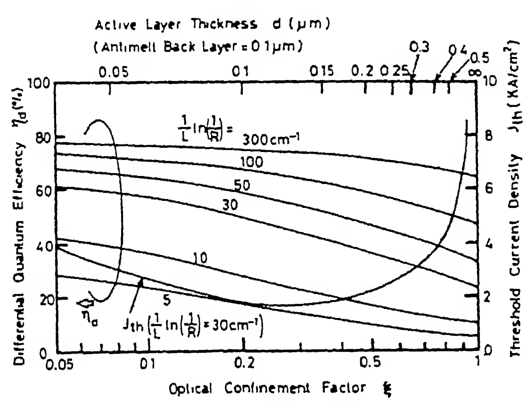

Calculation results of the differential quantum efficiency η_d (pulsed) of a 1.6 μm wavelength laser as a function of optical confinement factor ξ, for different mirror loss $\ln(1/R)/L$. Threshold current density J_{th} (pulsed) in the case of 0.1 μm thick antimeltback layer and $\ln(1/R)/L = 30\ cm^{-1}$ is also shown.

discussed by measuring the carrier lifetime,the loss, and the gain.The intervalence band absorption decreases the differential quantum efficiency, and both the nonradiative recombination and the carrier leakage over the heterobarrier decrease the carrier lifetime, and at the same time, increase the threshold current.Both effects of the absorption and the nonradiative components contribute significantly to the temperature characteristics.If we assume no absorption loss due to the intervalence band absorption, the exponential temperature coefficient T_o is estimated 145K.The rapid increase in the temperature-I_{th} curve with T_o=60K is due to the rapid inctrese of absorption.The heating effect due to the injection current also influences significantly the I_{th}, and the possible maximum temperature of lasing operation can be increased by decreasing the structural parameters such as the series resistance, the heat resistance and the threshold current.

OPTOISOLATORS

2.3.0. INTRODUCTION:

The optoisolator (or optron) is an optoelectronic device consisting of two basic components,namely a light source and a photodetector optically and structurally coupled together.This device is known as a photocoupled isolator, photocoupler, photon-coupled pair (PCP), photorelay.

2.3.1. OPERATION:

Any type of optron operates on the principle of double energy conversion:the radiator converts the energy of an electric signal to optical radiation and the photodetector does the

reverse-converts this radiation to electric current or or voltage.The optron thus has an electric input and an electric output for electric connection to an external circuit.Inside the device,however,the connection between the input and the output is optical:optical signals provide optical coupling(and thus electric isolation) between the radiator and photodetector,hence the name of the device a photocoupler or a photocoupled isolator.The optron can provide optical control of electronic circuits and thus enables the designer to evolve devices with unique parameters and characteristics.

As a circuit component designed to perform definite functions, the optron is primarily defined in terms of what type of photodetector it incorporates.It is the photodetector that determines the circuitry featurs of the optron.The principal physical advantages of optrons follows from the utilization of photons as carriers of information.These devices feature a very high input output electric isolation which excludes output to input feadback, provide unidirectional flow of information and have a large bandwidth.

2.3.2.BLOCK DIAGRAM:

The generalized block diagram of an optron and the forms of energy converted in its individual stages are shown in fig.2.3.0.The input unit (IU)serves to convert the input signals to the form suitable for efficient operation of a light source (LS).The optical channel (OC), serves to transmit the energy of an optical signal from the light source to the photodetector (PD) with a minimum of loss and without distortion of the waveform of the optical signal.The channel should secure a minimum of

non-forward scattering to exclude the effect of radiation on other light sensitive elements of the device.It also sholud have a reliable shield against external radiation that can be responsible for false triggering of the optron.

The possibility in principle exists for controlling the parameters of the optical channel with the aid of electrooptic or magnetooptic effects is evident from the block diagram, which illusrates a control unit CU for OC.Control over the output signal can be made viaboth the electric input of the optron and the optical input of the photodetector.The photodetector must convert an optical signal to an electric signal with a minimum of loss of its information content, for which reason it should have a high responsivity and sufficient speed.Operation of the LS-OC-PD chain can obviously be effective only after securing the match between the spectral characteristics of all its elements.

The output unit (OU) shapes the output signal from PD to a standard form convenient for its transfer to the subsequent stages, which are most commonly analog and digital microcircuits or semiconductor switches.Foe all links of the optron, the efficiency of energy conversion and speed are main criteria.The elements must alsointerfere adequately.Ensuring the match and compatibility of elements is the central task of optimum design of optrons

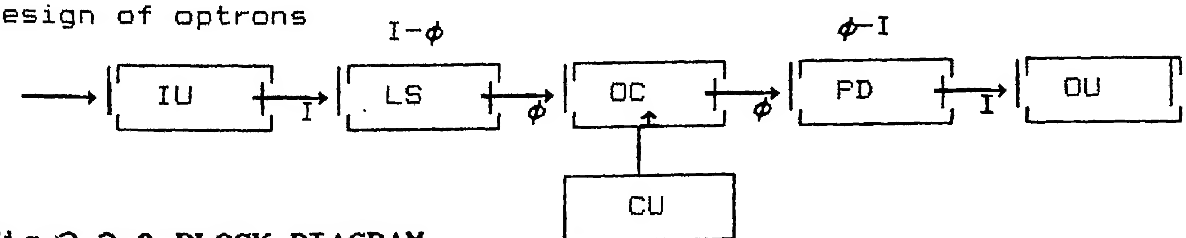

Fig.2.3.0.BLOCK DIAGRAM

2.3.3.TEMPERATURE DEPENDENT PARAMETERS OF OPTRONS:

The basic parameter of an optron is the current transfer

ratio (CTR),(denoted by K) which is temperature dependent, and this characterizes the signal transfer from the input to the output circuit of an optoisolator.This is the gain defined as the ratio of the output current to the input current: [12].

$$K = I_o/I_i \qquad (2.3.0)$$

when the leakage current I_{lk} at the PD output is comparable in magnitude with the output current, for example, in operation at high temperature, a correction for I_{lk} should be introduced into (2.3.0) to calculate the current transfer ratio

$$K = (I_o-I_{lk})/I_i \qquad (2.3.1)$$

The I_o-I_i relatio, which is known as the transfer charcteristic, is generally nonlinear for optrons.Formulas (2.3.0) and (2.3.1) define the static CTR .The differential CTR is given by

$$K_{diff}=\lim_{\Delta I_i \to 0} \Delta I_o/ I_i= dI_o/dI_i \qquad (2.3.2)$$

The static CTR is proportional to the slope α of a straight line drawn from the origin to the point of intersection on the I_o-I_i transfer curve i.e, (see fig.2.3.1)

$$K \sim \tan\alpha$$

The differential CTR is proportional to the slope β of the straight line tangent at the given point to the transfer curve i.e,

$$K_{diff}=\tan\beta.$$

The nonlinearity of the transfer characteristic tells us that the CTR varies with the input current.This is because the photoemission characteristic deviates from the linear pattern and the amplifier gain varies with the output current.

The temperature dependence of the CTR of an optron may be utilised to make sensors for the measurement of temperature. The strong temperature dependence of K due, mainly, to variations in the photoemitter parameters with temperature T; in the temperature range from -60 to 85°C, the K-T relation which is shown in fig.2.3.2 is practically linear and the temperature coefficient of K, %/°C, is equal to

$$(dK/dT)/K \simeq -0.5$$

This linearity helps us to exploit optrons for use as temperature sensors.

CHAPTER 3

EXPERIMENTAL RESULTS AND DISCUSSION

3.0.0. INTRODUCTION:

The temperature dependence of the characteristics of a p-n junction have long been utilised for measurement of temperature. In the middle seventies, the idea was further extended and a custom tailored integrated circuit (IC) was designed which processed the on-chip temperature dependent signal emanating from a silicon diode and presented it at the output in a very convenient form. This temperature sensing IC is now commercially available from vendors. One limitation of this IC, however, is that it is not immune to electromagnetic interference(EMI). To overcome this limitation, one can use the temperature dependent output of p-n junction based light emitting diodes (LEDs) or semiconductor lasers for temperature measurement. Experimental results are presented and discussed in the following sections.

3.1.0. USING HIGH RADIANCE LEDs:

LEDs can be roughly divided into two groups: high radiance devices and low radiance devices. High radiance devices which are used in optical fiber communicatin systems have, generally, pigtails available on them so that coupling of light output to the detector becomes convenient. Hence these were tried first. In priciple the devices worked well, but degradation of the devices over only a few cycles of operation was very severe. Hence with the present state of the art of fabrication and reliability of

high radiance LEDs the fabrication of temperature sensors does not appear to be feasible.Hence low radiance LEDs are considered for use as temperature sensors.

3.1.1. USING LOW RADIANCE LEDs:

The temperature dependence of the output power of LEDs is exploited to fabricate temperature sensors.Commercially available LEDs, such as GaP:N (green), GaP:Zn,O (red), $Ga_{.7}Al_{.3}As$ (red), $GaAs_{.6}P_{.4}$ (red) are considered in this study.Though LEDs of the same colour may be fabricated from different materials, it is important to know the exact material from which a particular device is made.The peak wavelength is different for LEDs made from different materials.Similarly the other characteristics are also different for LEDs made from different materials.

3.1.2. MEASUREMENT OF ELECTROLUMINESCENT SPECTRUM:

In order to know the peak wavelength, the electroluminescent spectrum of the LED is measured.Fig.3.1.0 **[13]** shows the experimental setup for measuring the emission spectrum.The recorded spectra of LEDs of different materials are shown in fig.3.1.1.The peak wavelength is noted from these spectra and the corresponding material from which the LED made is identified using Table-3.1.At present we are interested in the green and red LEDs made from the materials mentioned in section-3.1.1.So the temperature aging tests are performed separately and discussed below.

3.1.3. GREEN LEDs:

The LEDs under test are properly placed in an electric oven, so that the ambient temperature is uniform.The power output of the LED is measured using a fiber optic multimeter which displays

the power in dBm or dBμ.The temperature is increased with the help of the thermostat setting and the corresponding change in the power output is noted.Fig.3.1.2 shows the degradation of the output power of GaP:N LED with temperature at a constant driving current of 15 mA.The reasons for this degradation were mentioned already in chapter-2.From the figure it is observed that the power output decreases very little (about .3 dBm) upto a temperature of 70°C and then degrades rapidly.The power output change over a temperature range of 20-120°C is only 1.6 dBm and the degradation is not uniform.The experiment is repeated for different samples and the similarity of the characteristics was noted.

3.1.4. RED LEDs:

After identifying the LEDs of different materials from which they are made of, the temperature stressing test is performed separately for each device.Fig.3.1.3 depicts the power output versus temperature relation for GaP:Zn.O LEDs which are driven at a constant current of 15 mA.We observed a maximum power change of 6 dBm over a temperature range of 30-140°C.The degradation is more or less uniform.

The same experiment is repeated for GaAsP LEDs.Fig.3.1.4 shows the power output variation with temperature at a constant current of 15 mA.Though the degradation curve is similar in shape to that of GaP:Zn,O the power output change is slightly less.Over a temperature range of 30-140°C a power degradation of 4.75 dBm was observed.

Finally GaAlAs red LEDs are used in the temperature aging test at a fixed current of 15 mA.Fig.3.1.5 shows the observed

relation of power output versus temperature.It is similar in shape to the other two types of red LEDs but the change of power output (4.5 dBm) is slightly less over the same temperature range of 30-140°C.An LED should have a large power o u tput change with temperature in order to use it as a temperature sensor

3.1.5. SUITABILITY OF DIFFERENT TYPES OF LEDs AS TEMPERATURE SENSORS:

After discussing the relevant characteristics of LEDs for temperature measurement, now it is left to discuss which of them meets the requirements.From fig.3.1.2 it was observed that GaP:N LEDs will not meet the requirements of a temperature sensor.Here neither the degradation is homogenius nor the power output change is large.So these green LEDs do not appear to be suitable for temperature measurement.

Fig.3.1.6 shows the combined gragh of the power output versus temperature for all the red LEDs considered in this experimental study.All the three type show uniform degradation and the curve is linear over the temperature range of 30-140°C.But the maximum power change is not same for all of them.GaP:Zn,O has got more power output change over the temperature range of interest.

Secondly GaAlAs red LEDs have lower power change over the same range of temperatures considered for GaP:Zn,O LEDs.Also the output power is less for the driving current mentioned in fig.3.1.6.Finally GaAsP LEDs have relatively medium power change over the temperature range of 30-140°C.And the output power is in between those of GaP and GaAlAs red LEDs.

Above discussion shows that GaP:Zn,O LEDs appears to be

suitable as temperature sensors after proper calibration.Ofcourse the possibility of using GaAsP,GaAlAs red LEDs as temperature sensors is not ruled out.If we can overcome some of the problems faced in the experiment, then any or all of the red LEDs may be suitable as temperature sensors.

3.1.6. PROBLEMS FACED IN THE EXPERIMENT:

From the experimental results presented in the previous sections, it appears that the use of LEDs as temperature sensors is feasible.We can make those results even more promising, if we can eliminate some of the problems faced in the experimental study.Each of the problems are discussed below.

A: COUPLING OF POWER:

The radiation pattern of a visible LED is lambertian or nonlambertian depending on the type of packaging.In the lambertian radiation pattern, the luminous intensity varies as the cosine of the off-axis angle,θ.

$$I(\theta)=I_o \cos\theta$$

So the power is distributed along a range of angles from the off-axis.This is an essential requirement when LEDs are used as indicators, to have maximum sensitivity.But this is a handicap for our present purpose, where our concern is to couple maximum power from the LED into the fiber.

Coupling of power can be improved if connectors compatible to fiber connectors are designed for visible LEDs during the manufacture itself.Effective coupling of power emitted from a visible LED to a fiber can be achieved if we can place the LED in a metallic case to which a compatible fiber connector is joined.The metallic case can be of the similar type that used for

the insertion of high radiance LEDs.Proper epoxy bonding should be provided so that the LED will not be disturbed during operation, which otherwise would cause variations in the coupled power.The following diagram shows the required connector model.

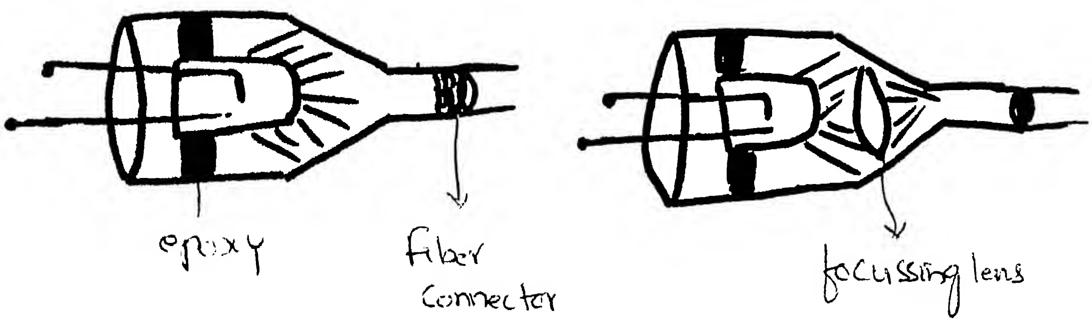

Another scheme can be suggested where a focussing lens is placed between the LED and the fiber tip.This gives better coupling of power to the fiber.

B: DETECTION:

The LED output power is measured using fiber optic multimeter in this experiment.This multimeter has a silicon photodiode sensor head of active area .38 cm^2 and the associated circuitry.The detector responds to a range of wavelengths of 400-1150 nm.The calibration setting was done at 900 nm for this sensor head, and so the response of the detector is good at this wavelength.where as the wavelenghths of the LEDs used in the experiment ranges from 550 to 700 nm.Accordingly the response of the detector is limited.In order to achieve best results, the detection scheme corresponding to each source has to designed separately.

C: TEMPERATURE DISSIMILARITY:

The ambient temperature of the LED was measured with the

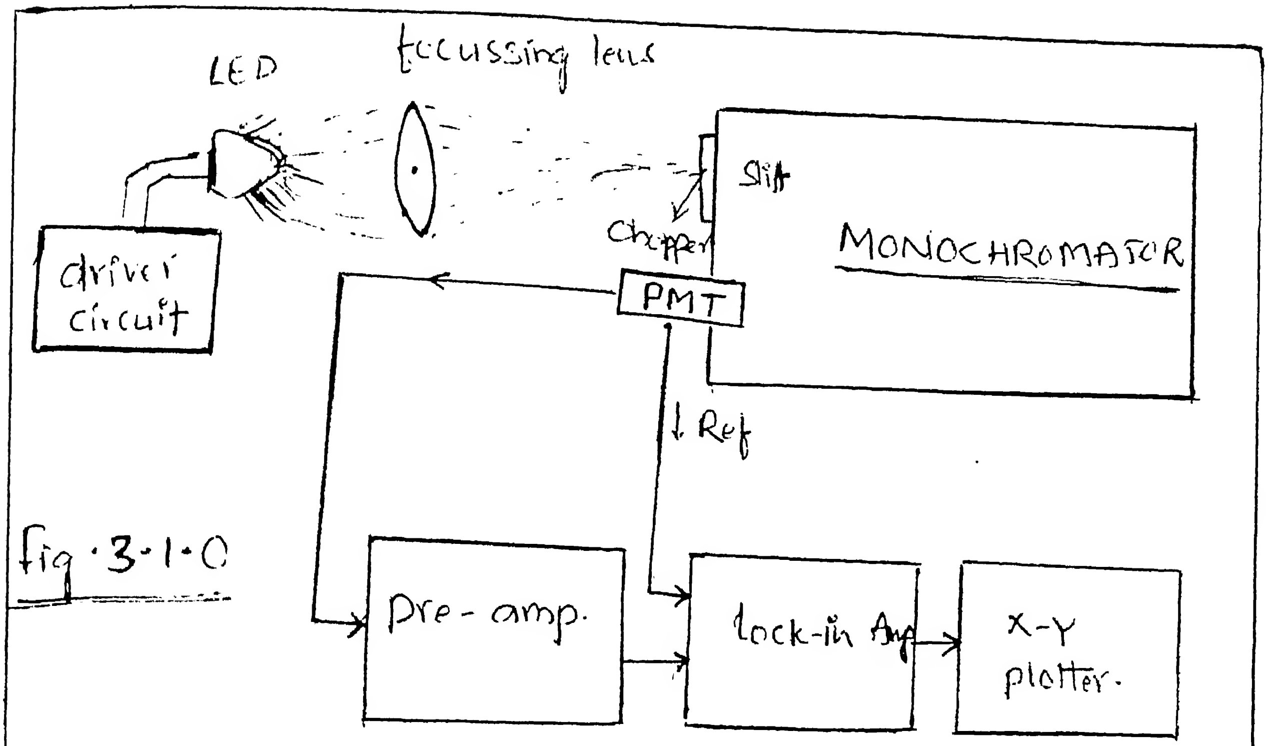

fig. 3.1.0

Measurement of Electroluminescent spectrum of LED

TABLE - 3.1

LEDs	Colour	Peak emission wavelength (nm)	Luminous output (lumens/watt)	External quantum efficiency: Best (%)	External quantum efficiency: Commercial (%)	Best luminous efficiency (lumens/watt)	Commercially available
GaP:Zn,O	Red	699	20	15	2.0-4.0	3.0	Yes
GaP:N	Green	570	610	0.7	0.05-0.1	4.2	Yes
GaP:NN	Yellow	590	450	0.1	0.05	0.45	Yes
$GaAs_{0.6}P_{0.4}$	Red	649	75	0.5	0.2	0.38	Yes
$GaAs_{0.35}P_{0.65}$:N	Orange	632	190	0.5	0.2	0.95	Yes
$GaAs_{0.15}P_{0.85}$:N	Yellow	589	450	-0.2	0.05	0.90	Yes
$Ga_{0.7}Al_{0.3}As$	Red	675	35	1.3	-	0.45	No
$In_{0.42}Ga_{0.58}P$	Amber	617	284	0.1	-	0.28	No
SiC	Yellow	590	500	0.003	-	0.01	No
GaN	Blue	440	~20	0.005	-		No
GaN	Green	515	420	0.1	-		No
GaAs:Si with YF_3YbEr	Green	550	660	0.1	-	0.6	No
GaAs:Si with YF_3:Yb:Tn	Blue	470	60	0.01	-	0.006	No
ZnSe	Yellow	590	450	0.1	-		No

Fig. 3.1.1 Measured Electroluminescent Spectra of some LEDs

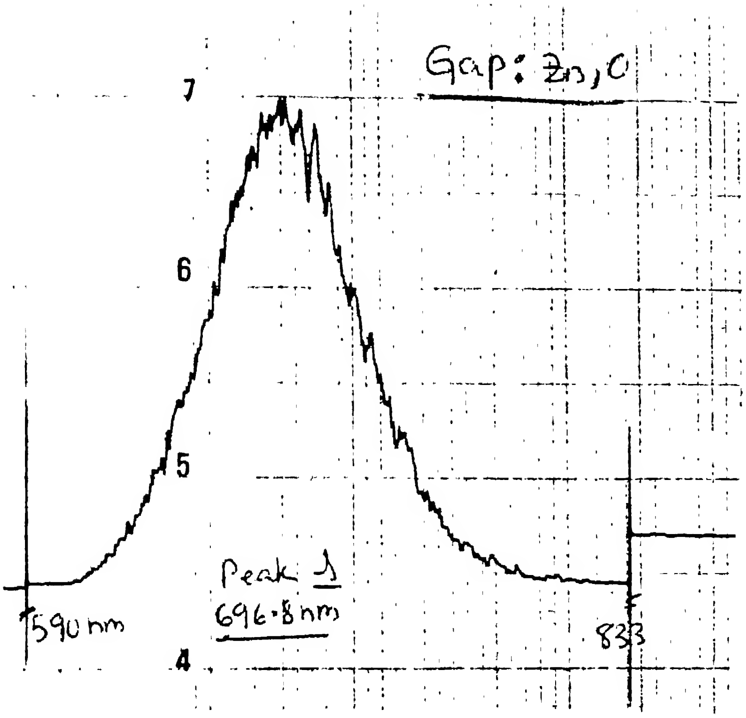

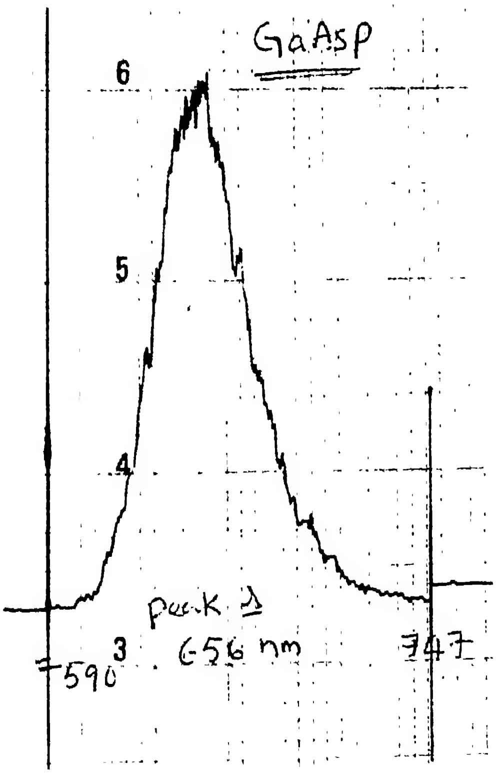

Fig 3·1·2 (GaP:GREEN) LED OUTPUT POWER Vs TEMP.

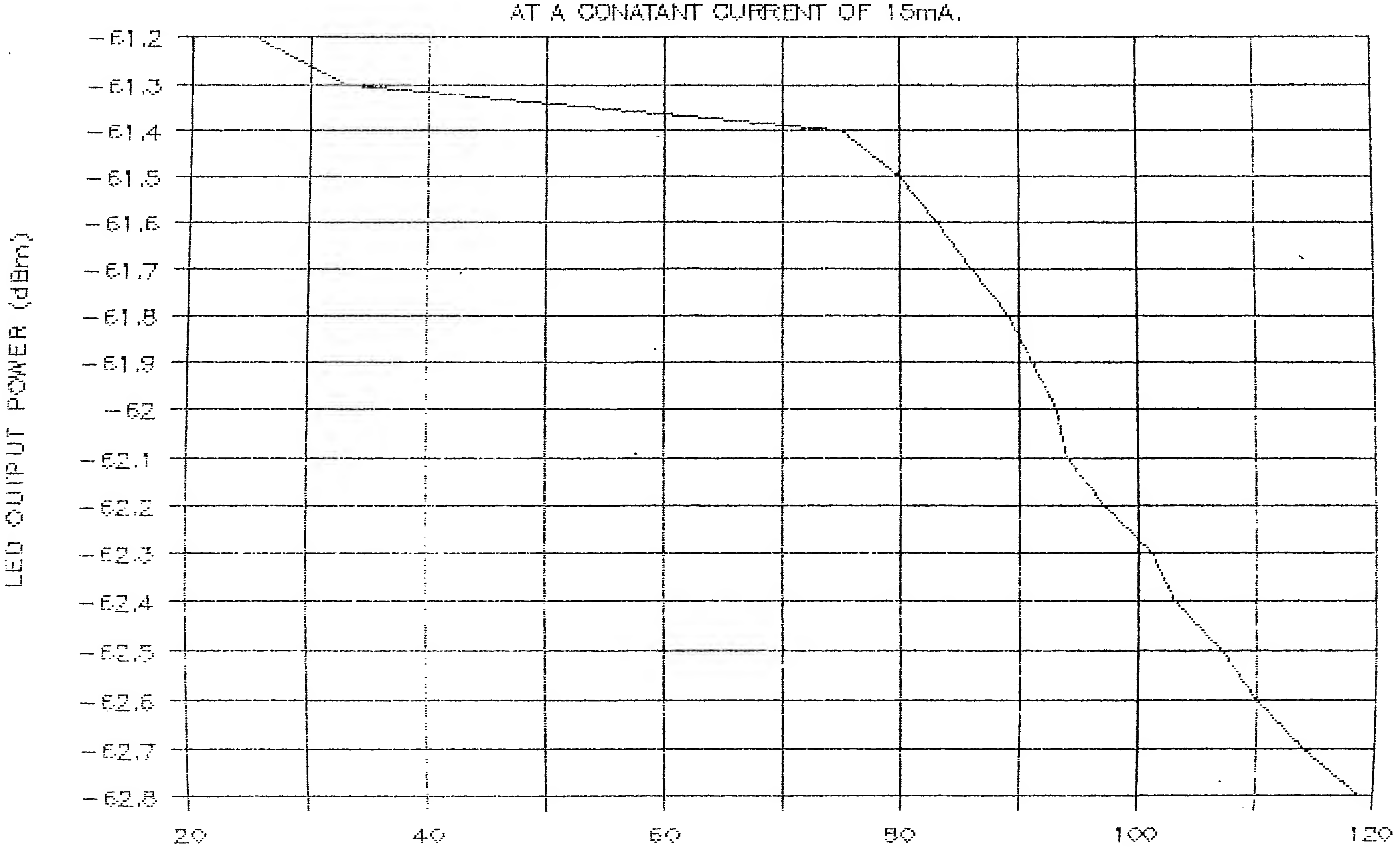

fig 3·1·3 (GaP.RED) LED OUTPUT POWER Vs TEMP.

AT A CONSTANT CURRENT OF 15mA.

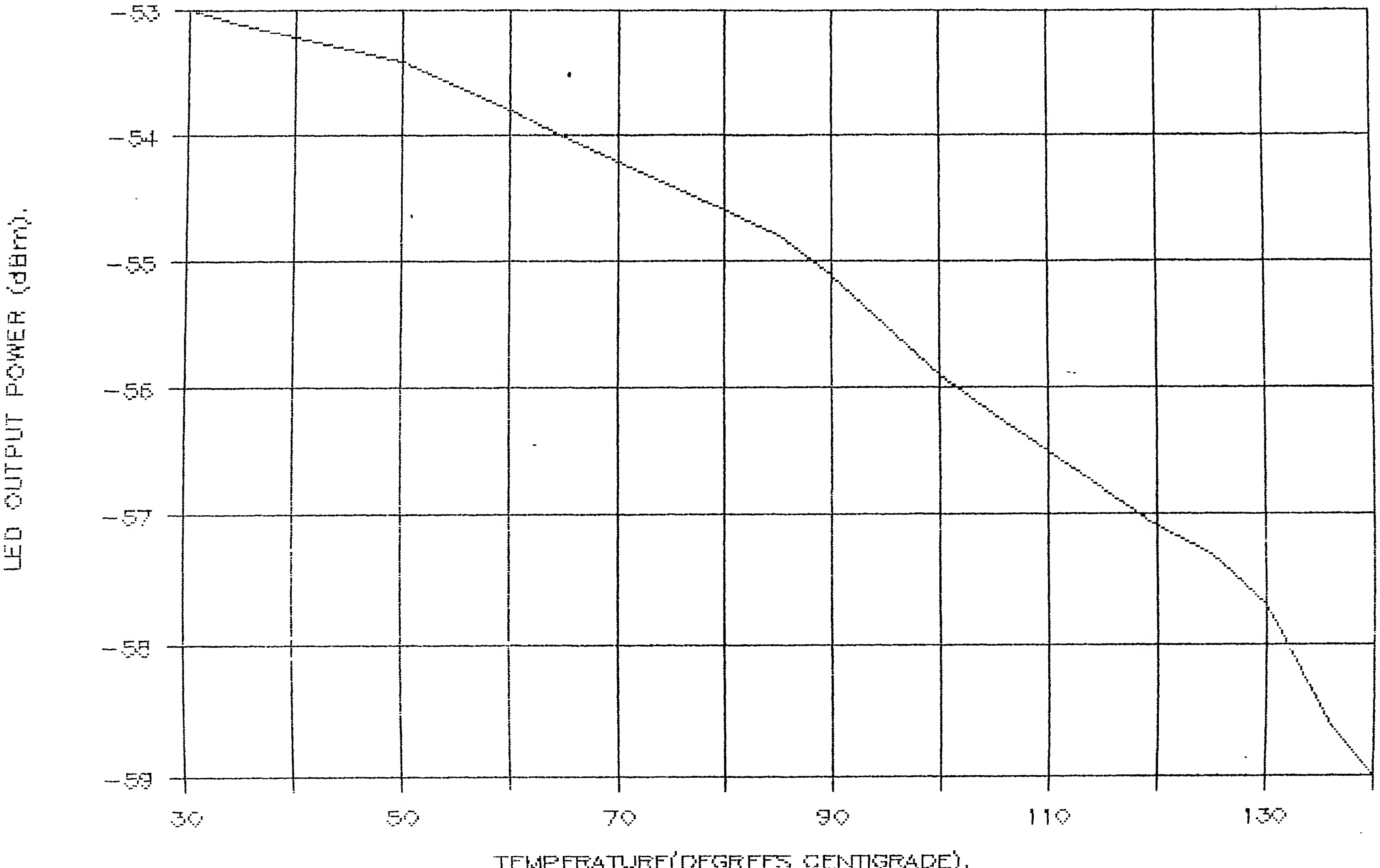

Fig. 3.1.4 (GaAsP:RED) LED OUTPUT POWER Vs TEMP.

AT A CONSTANT CURRENT OF 15mA.

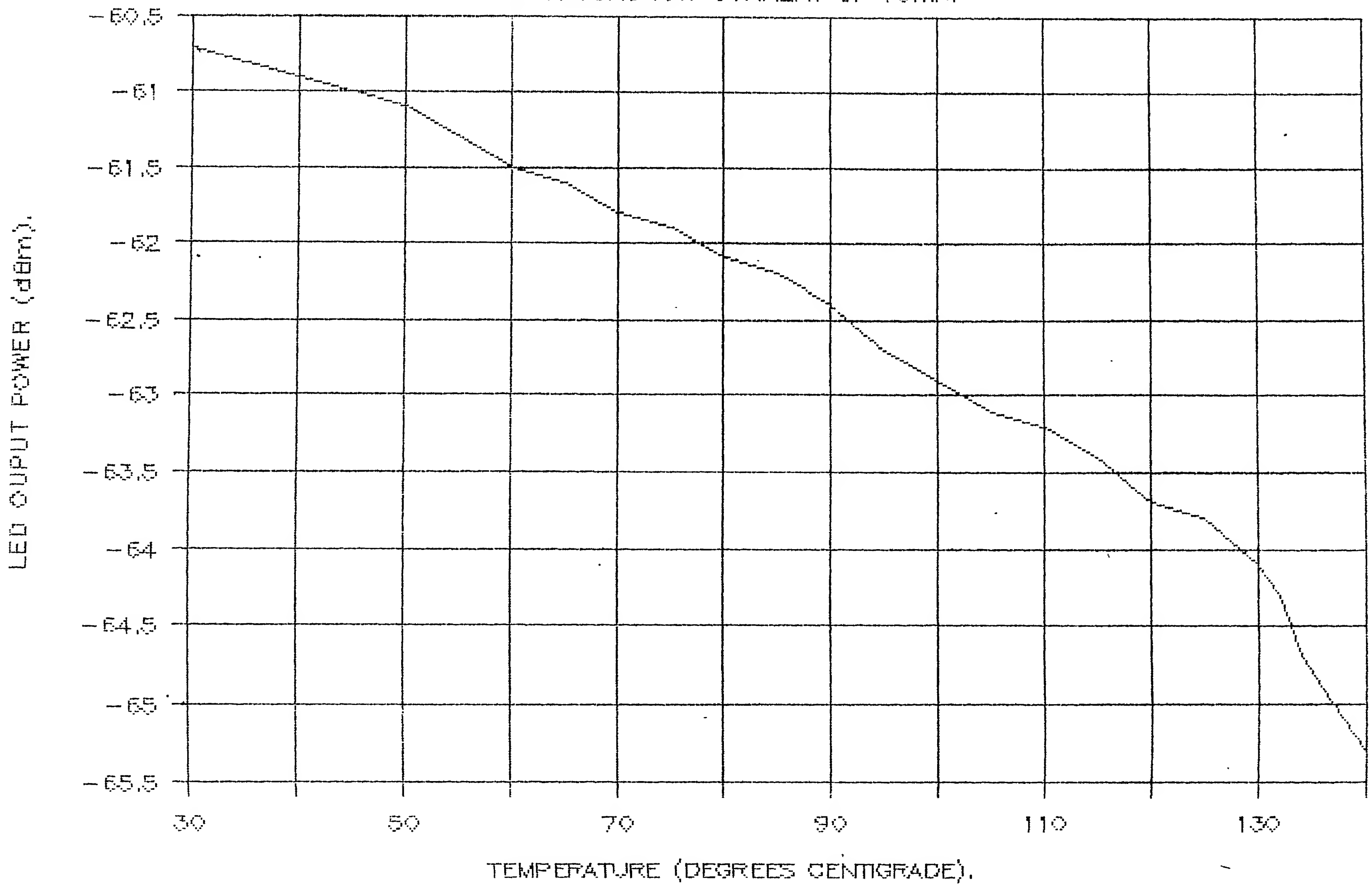

Fig 3.1.5 (GaAlAs:RED) LED OUPUT POWER Vs TEMP.

AT A CONSTANT CURRENT OF 15mA.

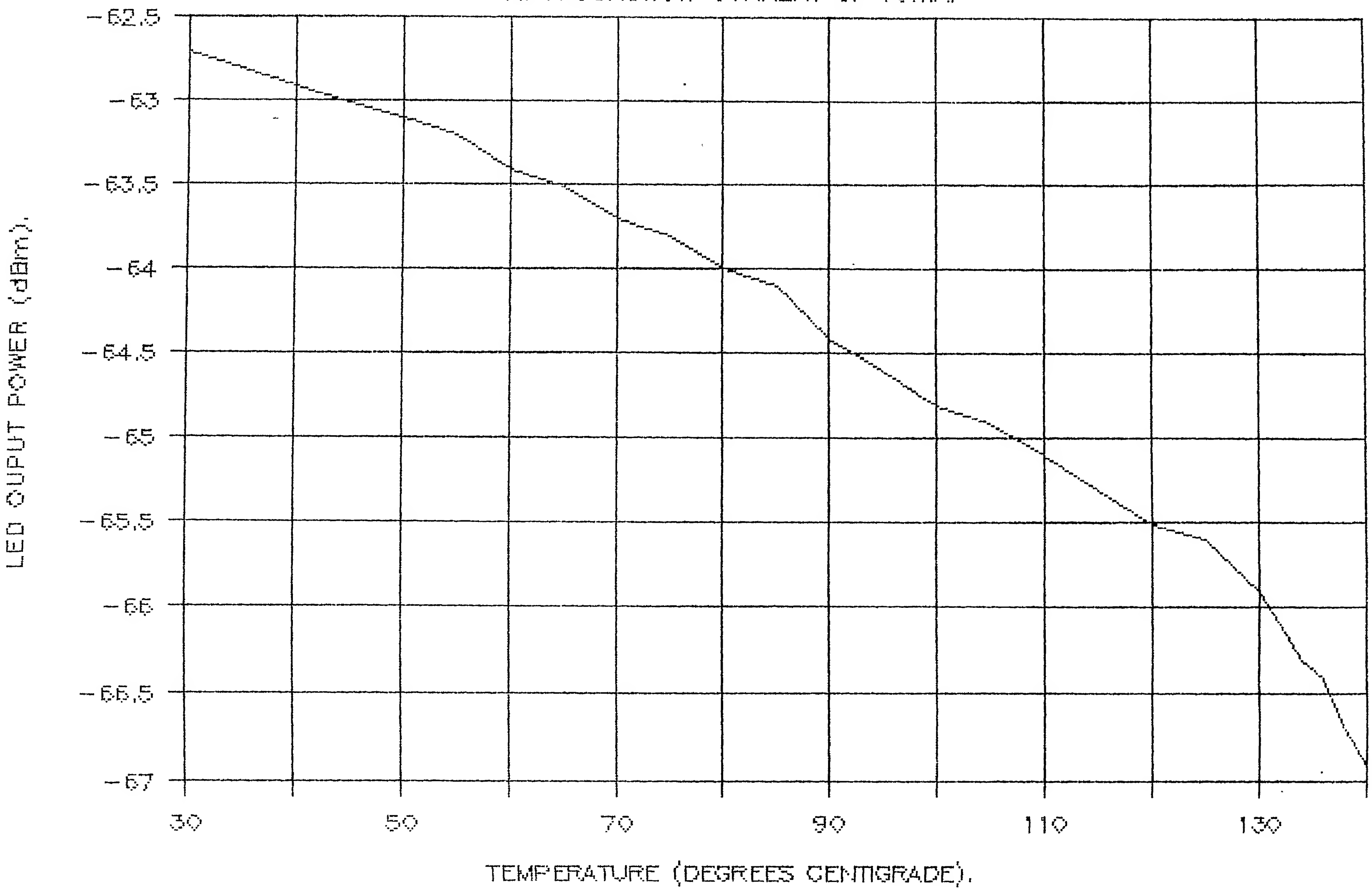

fig.3.1.6 LED OUTPUT POWER Vs TEMP(CURRENT=15mA)

(TOP=GaP,MIDDLE=GaAsP,BOTTOM=GaAlAs)

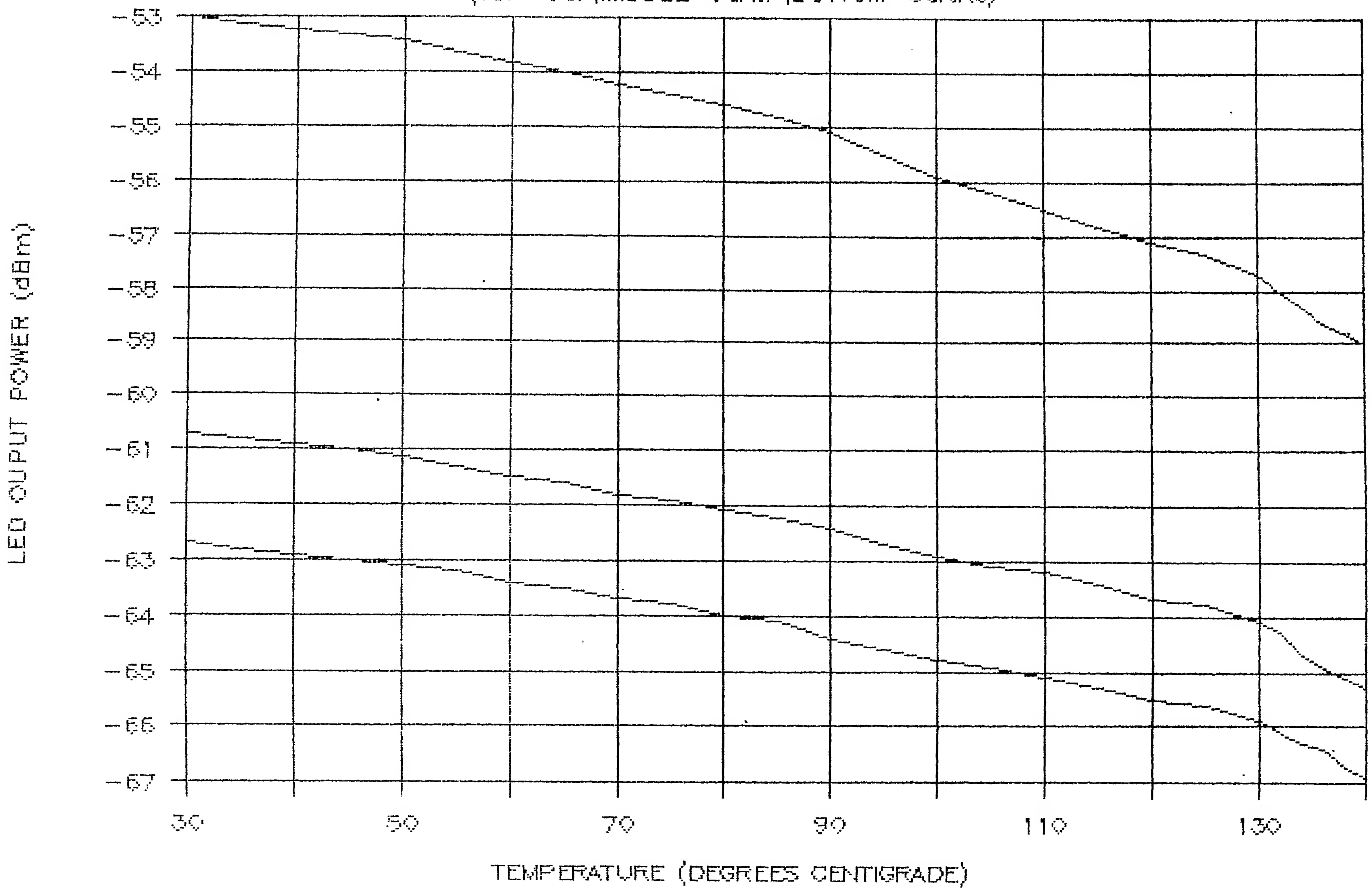

help of the built-in L-shaped thermometer, which appears on the front portion of the electric oven.We measured the same temperature with the help of a semiconductor temperature transducer as well, and noticed a variation of ±1°C from that of the thermometer reading .There was no exact similarity in the readings of both the thermometer and the semiconductor sensor.The semiconductor temperature transducer has a current change of 1μA/°K.Since we are interested in the relative change of temperature, any one of the above two methods may be used for the measurement of temperature.The difference in the temperature reading might be due to variation of power supply, which can cause significant changes in current and there by temperature.

D: CONNECTOR DAMAGE:

As the temperature is increased well above 100°C, the delicate plastic material which is wound around the connector end begins to expand and ultimately results in the damage of the fiber connector.In order to overcome this problem.the connector end may be wrapped with a high melting point synthetic material.

E: IDENTIFICATION OF MATERIAL:

If an LED gets damaged, then we can not simply replace the same from the market.Though the colour is same, they are made of different materials the peak wavelength of which is different.So for each LED, the peak wavelength has to be measured and the material is identified before inserting it in the sensor circuit.

SEMICONDUCTOR LASERS

3.2.0. MEASUREMENT OF THRESHOLD CURRENT (A):

It is useful to consider the behaviour of double heterojunction (DH) lasers as the current is increased from the low current densities of spontaneous emission to currents in excess of the laser oscillation threshold.A detection scheme for the measurement of the laser diode emission intensity for determining the threshold current is shown in fig.3.2.0.The output current of the reverse biased Si detector is given by the voltage across the 50Ω resister.If this current is divided by the detector conversion efficiency η_c (η_c=.7) for most silicon detectors at wavelengths between 0.8 and 0.9 μm), then the current $I_D = 2V/\eta_c 50$ and when divided by the charge q gives the no.of photons emitted from the two faces of the Fabry-Perot cavity.The factor 2 in the above equation accounts for the emission from both faces.This output current I_D is plotted in fig.3.2.1 as a function of the laser diode current I_L for a DH laser.

This broad area laser with sawed sides is 130 μm wide and 360 μm long with a 0.1μm active layer.In the example shown here the laser is not mounted on a heatsink and is excited with a 0.1μs low-duty cycle pulse to prevent heating.

As I_L is increased the spontaneous emission linearly increases for currents up to 0.45A and I_D then abruptly increases near 0.5A as laser oscillation begins.The extrapolation of this curve to zero I_D, as illustrated by the dashed line gives the threshold current I_{th}.The threshold current density J_{th} is I_{th}/a where a in this case is 4.7×10^{-4} cm^2, J_{th} is 10^3 A/cm^2.The commonly used procedure is to measure I_D only at currents in excess of threshold current as illustrated in fig.3.2.1 to obtain

I_{th}.Another useful quantity that may be obtained from this plot of I_D versus I_L is the differential quantum efficiency η_d, which is defined as

$$\eta_d = \Delta I_D / \Delta I_L.$$

The threshold current measured in this way agrees closely with the manufacturer's specification value.

3.2.1.MEASUREMENT OF THRESHOLD CURRENT (B):

The threshold current of a semiconductor laser can be measured by another scheme.The experimental setup is shown in fig.3.2.2.The laser that can be used in the experiment is a DH GaAlAs or InGaAsP laser.The stimulated emission is detected by a photodetector.The detector output after amplification is fed to the comparator.The other input to the comparator is a reference voltage which is fixed depending upon the light output from the laser.The light output is different for different settings of threshold current.

Suppose if we fix the threshold current say at I_{th1}, then corresponding to this I_{th1} there will be a light output ϕ_1 as shown in the fig.3.2.3.Based on this output the reference voltage is fixed.So whenever the laser reaches its threshold the voltage at the comparator +input is equal to the reference voltage at the comparator -input.At this point the comparator changes its state either to low or high depending on its input connections.The logic circuit included in the loop disables the counter which enables the user to decode and display it using a seven segment display.The output of the counter is used to drive the laser after it is converted to an analog output using a digital-to-analog (D/A) converter.A current source may be

included after the D/A converter, which is essential to drive the laser to higher currents.

Preliminary measurement of threshold current can be made using the aforementioned procedure.Now the semiconductor laser is placed in an electric oven and its temperature is raised.Depending upon each setting of threshold current, there will be a temperature at which the comparator changes its state.The experiment is repeated for several settings of the threshold curent.Fig.3.2.4 shows the typical variation of light output of the laser versus driving current at different temperatures.

Lasers will not maintain a constant optical output if the device temperature (more specifically, the junction temperature) is changed.The threshold currents of typical lasers change by approximately +1%/°C.The 1%/°C is far more disastrous in terms of output stability as its effect is magnified by the high differential quantum efficiency beyond threshold.In a typical laser, a change of only 30°C, results in a complete loss of lasing output for levels below 5mW.The relationship between the measured threshold current and the heatsink temperature of the semiconductor laser is shown in fig.3.2.5

3.2.2. PURELY ELECTRICAL MEASUREMENT OF THRESHOLD CURRENT:

A: STATIC LASER CHARACTERISTICS:

The relationship between output power P and drive current I for a semiconductor laser diode is given by, [14]

$$P = (\eta h\nu/q)(I-I_{th}) \qquad (3.2.0)$$

where $h\nu$ is the lasing photon energy, q is the electron charge, η is the external differential quantum efficiency.Below threshold

the lasing power is zero.If I_{th} is assumed to be constant then the P-I curve is linear.However, it is found that practical cw lasers have P-I curves that are some times nonlinear.These nonlinearities in P-I curves are frequently due to instabilities of the optical lasing mode.

The nonlinearities discussed here result from junction heating which produces a floating value of I_{th}.Assuming that $I_{th} \alpha \exp(T/T_o)$ where T_o is a characteristic parameter, the threshold current increase for a ΔT temperature change is

$$I_{th} = I_{tho} \exp(\Delta T/T_o) \qquad (3.2.1)$$

ΔT is proportional to the drive current because of the power dissipation in the laser.In the absence of heating,$I_{th} = I_{tho}$, the nominal threshold current of the device.Experimentally, I_{tho} can be determined using low duty cycle pulses where heat generation is negligible.

If V_j [$\simeq E_g/q$] is the junction voltage,R_s is the series resistance, and I the driving current then the power dissipation Q in cw operation is

$$Q = (1-\eta_p)(V_j I + R_s I^2) \qquad (3.2.2.)$$

where η_p is the power efficiency.Because $\eta_p \leq 10\%$ in typical devices it will be neglected.Consequently the tempearture rise ΔT above the heatsink temperature is assumed to be $\Delta T \cong R_{tm}(V_j I + R_s I^2)$ where R_{tm} is the thermal resistance.The laser output P can be expressed as

$$P = (\eta h\nu/q) \left[I - I_{tho} \exp[R_{tm}(V_j I + R_s I^2)/T_o] \right] \qquad (3.2.3)$$

In cw operation the threshold current is a solution of

$$I_{th} = I_{tho} \exp[R_{tm}(V_j I_{th} + R_s I_{th}^2)/T_o] \qquad (3.2.4)$$

R_s is determined experimentally from the diode V-I characteristics, I_{th} and I_{tho} are found from the pulsed and cw P-I curve, and the ratio R_{tm}/T_o is from (3.2.4).

$$R_{tm}/T_o = \frac{\ln(I_{th}/I_{tho})}{V_j I_{th} + R_s I_{th}^2} \qquad (3.2.5)$$

B: ELECTRICAL MODEL FOR A SEMICONDUCTOR LASER:

Electrical characteristics of DH lasers have been a subject of considerable interest for many years.The electrical characteistics of these lasers are adequately represented by a resister in series with a p-n junction characterized by a classical diode equation,

$$I = I_s[\exp(qV_j/\eta kT)-1] \qquad (3.2.6)$$

Measurement of the first derivative dV/dI and the product IdV/dI is shown to be an especially useful technique for electrical characterization, yielding accurate and direct determination of the series resistance, the exponential junction parameter, and the laser threshold current.The observation of lasing threshold from an electrical measurement, instead of from the more usual optical measurement is discussed in terms of the saturation behaviour of the junction voltage at and above threshold.

The electrical model for a proton-bombarded stripe-geometry junction laser consists of an ideal p-n junction in series with a resistance R which accounts for the resistance of the bulk material and the contacts.Possible leakage paths around the junction, such as through the proton-bombarded material are represented by a shunt resistance R_{sh}.The equivalent circuit is shown in fig.3.2.6.

The I-V characteristics of this equivalent circuit is given by, [15]

$$I = \frac{V}{R_{sh}} + I_s\left\{ \exp\left\{[(1+R/R_{sh})V-IR]/\frac{\eta kT}{q}\right\}-1 \right\} \qquad (3.2.7)$$

where V is the applied voltage at the device terminals, I_s is the junction saturation current,and η is a parameter characteristic of the p-n heterojuction.The I-V relation of (3.2.7)can be recast into a form more suitable for measurement of the parameters η and R .

$$V = \frac{1}{1+R/R_{sh}}\left[IR+\frac{\eta kT}{q}\ \ln\left(\frac{I}{I_s}+1-\frac{V}{I_s R_{sh}}\right)\right] \qquad (3.2.8)$$

from which the differential resistance at current I is given by

$$\frac{dV}{dI} = \frac{R+\frac{\eta kT}{q}\,\frac{1}{\left(I+I_s-V/R_{sh}\right)}}{(1+R/R_{sh})+\frac{\eta kT}{q}\left[\frac{1}{(I+I_s)R_{sh}-V}\right]} \qquad (3.2.9)$$

The effect of shunt resistance is usually negligible above 10^{-7}A, while the current near threshold is in the vicinity of 100 mA.Hence this cumbersome equation can be reduced to

$$\frac{dV}{dI} = R+\frac{\eta kT}{q}\,\frac{1}{(I+I_s)} \qquad (3.2.10)$$

Furthermore for most cases of practical interest $I \gg I_s$ so that

$$\frac{dV}{dI} = R+\frac{\eta kT}{q}\,\frac{1}{-} \qquad (3.2.11)$$

I

Thus a plot of dV/dI versus 1/I is linear with a slope equal to $\eta kT/q$ and the intercept at 1/I=0 equal to R.An alternate form of the above equation, which is also suitable for direct mesurement is

$$I\frac{dV}{dI} = IR+\frac{\eta kT}{q} \qquad (3.2.12)$$

In this case, the productI dV/dI is linearly related to I with a slope equal to R and a zero-current intercept equal to $\eta kT/q$.

C: DERIVATIVE MEASUREMENT SYSTEM:

The first derivative of the V-I characteristics of DH lasers was measured and recorded with the system illustrated in fig.3.2.7.The ac current modulation was provided at 10kHz by an audio generator loaded with 250kΩ.The modulation amplitude was set at less than 10% of the minimum bias current to ensure a minimal contribution from the higher order terms.The ac voltage generated across the laser was detected with a lock-in amplifier whose output was multiplied by a signal proportional to the dc current and then recorded as a function of current.The system was calibrated by replacing the laser with accurately known resistors of value 1.0Ω and 4.3Ω.With each linear resistor,the output of the recorder was a straight line passing through the origin with slope equal to its resistance.A slight rearrangement of the components in fig.3.2.7 also allowed the derivative dV/dI to be recorded as a function of 1/I.

In this configuration, the lock-in output was sent directly to the recorder while the inverse of the current was taken by the multiplier before recording.Recording of dV/dI as function of 1/I is convenient in detecting changes in $\eta kT/q$ as a function of

current. A disadvantage is the nonlinear abscissa.

D: EXPERIMENTAL OBSERVATION:

An observation of the experimentally observed variation of IdV/dI with current is shown in fig.3.2.8. It is observed that the product IdV/dI decreases abruptly at a current in the vicinity of the lasing threshold. Well below threshold, IdV/dI varies linearly with current at a rate equal to the series resistance R, which for a typical laser, is 1.78Ω. Due to clipping by the lock-in amplifier, the measurement was not accurate below about 20 mA. However, extrapolation of the linear relation to zero current yields $\eta kT/q=0.0675$ or a value of 2.63 for η (T=298K).

Now increasing the temperature of the heatsink of the laser the above experiment is repeated. And for each temperature setting, the I(dV/dI) is plotted as a function of current. The results are shown in fig.3.2.9.

It is clear that the break point in the curve moves to higher currents along with the laser threshold. Furthermore over the temperature range studied, the value of $\eta kT/q$, measured by the zero-current intercept, scaled linearly with the absolute temperature indicating a relatively constant η for $10mA \leq I \leq 100mA$. Secondly, the lasing threshold was also measured by the current at which a saturation occured in the emission polarized orthogonally to the lasing emission. Threshold measured in this way agreed accurately with the current at which the product I(dV/dI) abruptly decreased.

Final confirmation that this abrupt decrease is a result of the onset of lasing was obtained by operating a diode first with and then without lasing. Since the threshold current determined

this way coincides with the threshold measured in conventional ways, it provides an accurate and reliable method of determining threshold by a purely electrical measurement.Furthermore,loss of the voltage saturation indicates the presence of a nonlinearity in the current dependence of the lasing emission.Thus this technique graphically and accurately reveals the range of currents over which the light output characteristic is linear and well behaved.

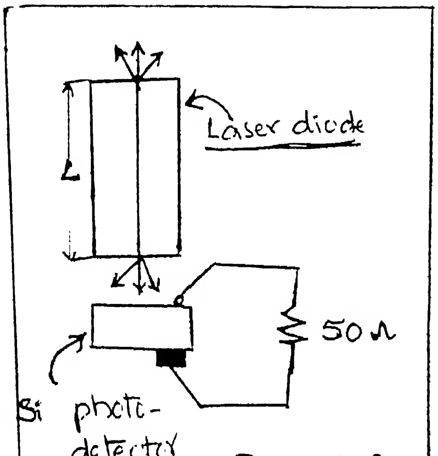

fig·3·2·0

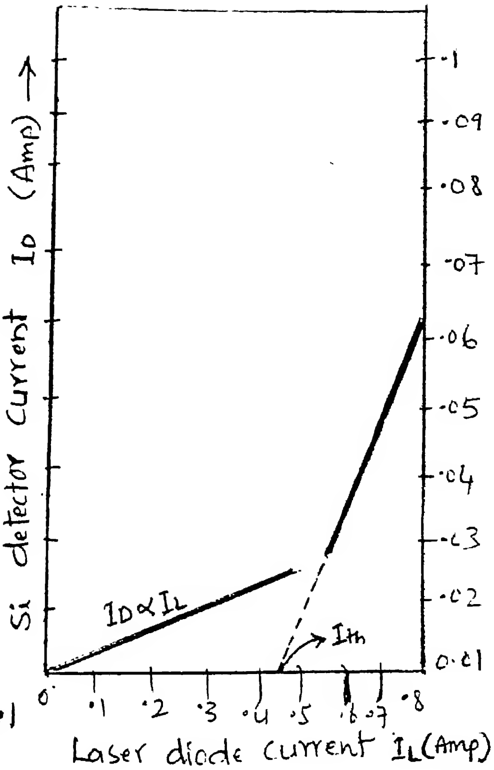

fig·3·2·1

fig·3·2·2. Measurement of Threshold Current

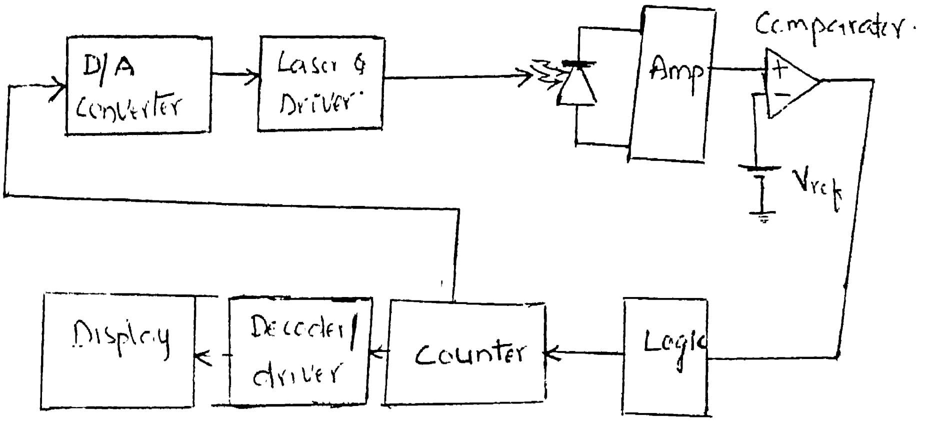

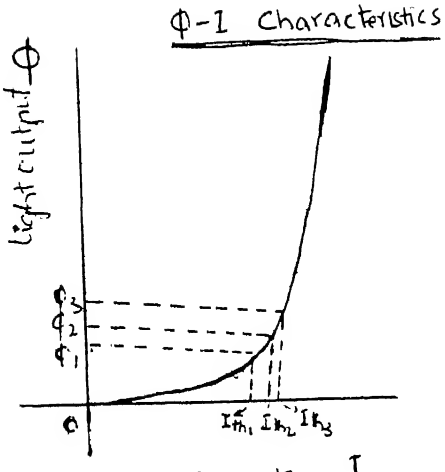

fig. 3.2.3

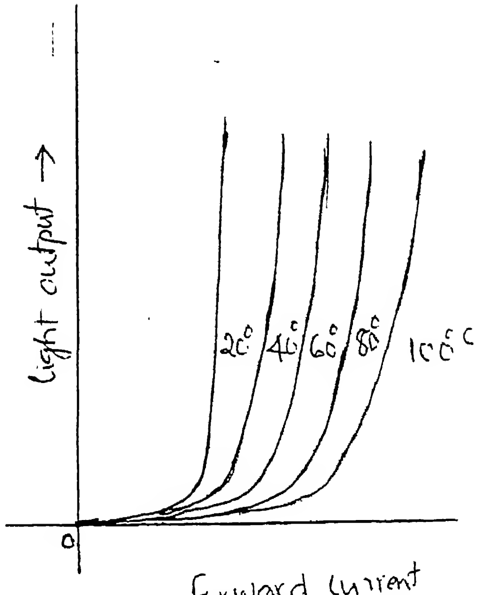

fig. 3.2.4

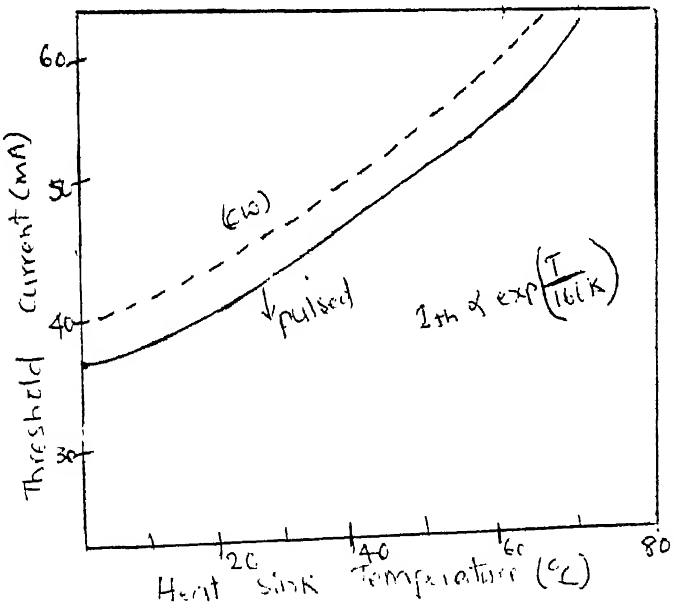

fig. 3.2.5

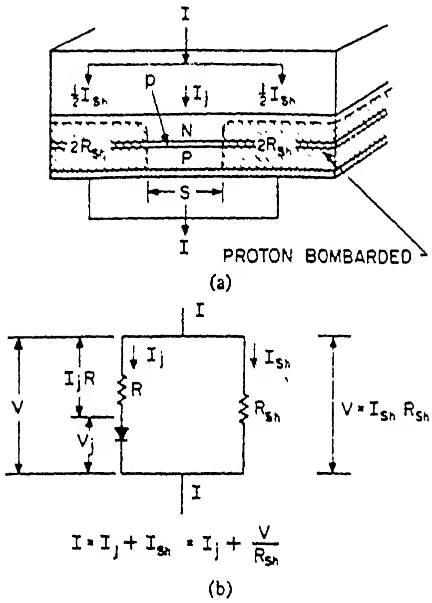

Physical structure (a) and equivalent electrical circuit (b) of a stripe-geometry, proton-bombarded DH laser.

fig 3·2·6

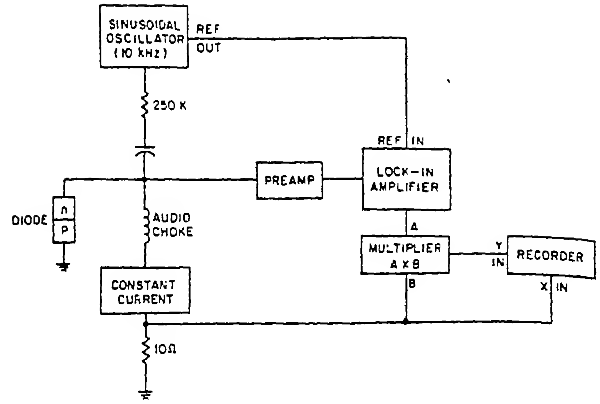

Block diagram of the circuit used to measure the first derivative dV/dI of a DH laser.

Fig·3·2·7

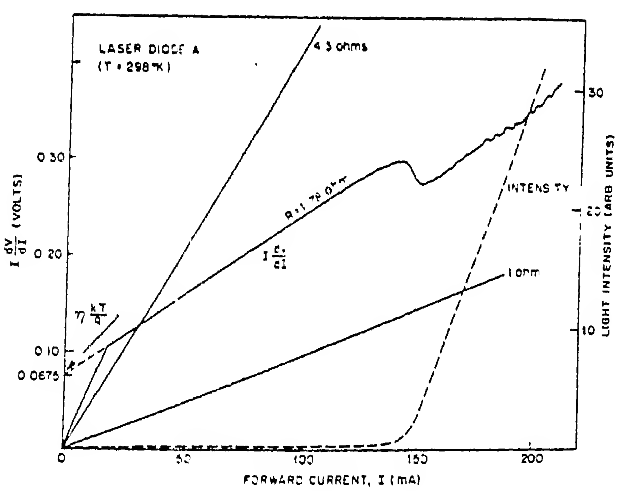

$I(dV/dI)$ versus I and laser light output versus current of laser diode A, indicating voltage saturation at I_{th}.

fig 3·2·8

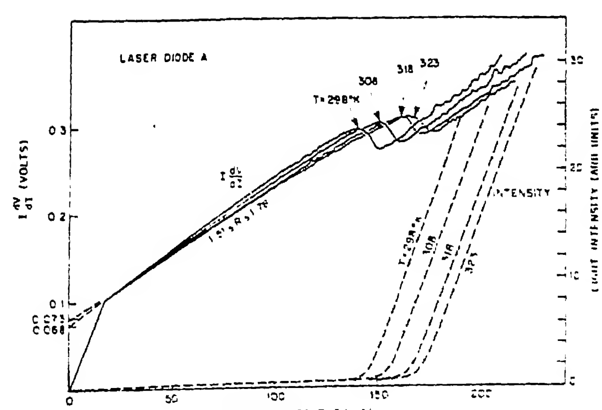

$I(dV/dI)$ versus I and laser light output versus current for laser diode A, as a function of temperature, near room temperature.

fig 3·2·9

CHAPTER 4

RELIABILITY ASPECTS OF LIGHT EMITTING DEVICES

4.0.0. INTRODUCTION:

The reliability of optical sources is strongly dependent on the degradation mode and device characteristics such as current versus optical output power and its temperature dependence. The influence of physical degradation on the degradation rate of the device characteristic s is effected by (or modulated by) the device characteristics themselves. For example the degradation rate of devices with poor temperature characteristics is faster than for devices with good characteristics. The reliability aspects of light emitting devices are briefly described in the following sections.

4.1.0. LEDs:

In recent years LED lifetimes have been extended so that they are now sufficient for most practical operatng conditions at ambient temperatures between 50° and 85°C. The reliability of an LED can be considered to be dependent upon two separate variable factors. These are the reliability characteristics of LED semiconductor chip and the reliability characteristics inherent to the package into which the chip is assembled. The variables are not necessarily independent because, for instance, package failure which is not in itself catastropic can trigger eventual failure or degradation of the semiconductor device.

From a theoretical standpoint, an LED like any p-n junction should have a nearly infinite lifetime. This operating lifetime

would be limited only by the infinitely slow natural diffusion of dopants. In practice, LED device operated under reasonable stress conditions is normally expected to exhibit an operating lifetime of about 10^5 hrs. The slow reduction of light output with time is a well known characteristic of an LED device. This degradation of light output exhibits a direct correlation to the current density in the junction. It is important to note that with increasing stress time, even those device lots which start out with a very high rate of degradation converge to a very low degradation rate. This implies that devices showing a high initial degradation will not necessarily continue to degrade to failure.

For an LED, the package is required to provide an optical system to enhance coupling of the emitted light to the detector and environmental protection to the device. Ideally designed and utilized package would perform these functions very rapidly. There are, however, many variables which can affect this performance. To evaluate a package, tests such as solderability, temperature cycling, thermal shock, moisture resistance, mechanical shock, acceleration and terminal strength are performed at various stress levels. These tests can be used to establish the worst case environmental stresses which should be applied to the package.

4.1.1: TEMPERATURE AGING AND PREDICTION OF DEVICE LIFETIME:

The generally accepted purpose of performing elevated temperature degradation studies, is to come to some reasonable estimate of the useful life of the device under its expected operating conditions. To this end, the accepted practice has been to verify that the temperature dependence of the degradation process under a given combination of stress and measurement

current is reasonably described by Arrhenius law:[16] (4.1.0)

$$t(T) = c \exp(E_A/kT). \quad (4.1.0)$$

Here t is some suitably defined characteristic time of the degradation process at absolute temperature T, E_A is an apparent activation energy which describes the temperature dependence of degradation, and c is a properly dimensioned constant of proportionality.Once this law has been verified to an acceptable degree over the elevated temperature range studies, the constants c and E_A are used to extrapolate the process down to the operating temperature.

Obviously the definition of the characteristic time used in Eq.4.1.0 is a critical point.One convenient choice is the mean time to failure (MTTF):the time at which the the average relative efficiency ($\langle\eta/\eta_o\rangle$) of the LED has dropped to a value of 0.5.Such a definition, by its very objectivity, effectively ignores all the structure observable in the time dependence of η/η_o, and heavily weights the first measurement of device efficiency and the measurements bracketing the η/η_o=0.5 point, ignoring all others.

An alternate definition of characteristic time takes advantage of the linear regions observed when $\log(\eta/\eta_o)$ is plotted as a function of $(\text{time})^{1/2}$.The lines defined by these linear regions do not, in general, pass through the point η/η_o=1 at t=0.This offset which varies from slice to slice, is termed the "rapid component" of degradation, as distinguished from the longterm linear region.Since MTTF is the parameter of interest in device operating life, its use is generally preferred as long as temperature dependence satisfies Eq.4.1.0.

Thermally accelerated aging tests can be performed for predicting the device lifetime.Fig.4.1.0 [17] shows the Arrhenius plot of elevated temperature stress data at a fixed driving current.This aging test is performed to obtain severe degradation with in a reasonable time scale.When extrapolated to normal operating conditions a device life of 10^7 hrs is predicted.

SEMICONDUCTOR LASERS

4.2.0. INTRODUCTION:

The degradation of laser diodes may result from mirror (facet) damage, the internal formation of nonradiative centers due to lattice defects, or an increase in the electrical or thermal resistance.Facet damage which is related to the optical flux density,is controlled by the use of Al_2O_3 facet coatings and by operating lasers at moderate power emission levels.The internal damage mechanism (gradual degradation) is caused by electron-hole recombination.It is generally accepted that the energy released in nonradiative electron-hole recombination enhances point-defect displacement leading to the accumulation of defects in the recombination region.The rate of this displacement process is expected to increase with temperature.Since gradual degradation is a process which depends on the electron-hole recombination rate, it occurs similarly in both the lasing and the incoherent emission state of diodes at comparable current densities.

4.2.1. ACCELERATED LIFE TESTING:

The systematic use of elevated temperatures is to compress the service life-span of an optoelectronic device into the time scale of a laboratory experiment.There are indications that

the method may be on the point of receiving a wider acceptance due to the ever increasing demand for higher and predictable reliability, and also,it must be said, for want of any better alternative.The basic philosophy of accelerated life testing is to operate devices at different degrees of overstress, in order to establish a relationship between device life and the amount of overstress.Estimates of device life under normal conditions are then obtained by extrapolation.The best example of this is temperature overstress life testing.The degradation process is taken to be thermally activated such that the time to failure (t_f) follows the Arrhenius relationship,

$$t_f \propto \exp(E_A/kT) \qquad (4.2.0)$$

where E_A ia an activation energy for the degradation process and T is the device temperature.Fig.4.2.0 [18] shows the τ_{laser}, the time needed for a 20% threshold current increase at various temperatures.The choice of this "figure of merit" is partly arbitrary because such a threshold increase need not terminate the life of a cw laser when the current is adjusted to keep the power output constant.

However, because such an increase does represent a very significant level of laser deterioration which is a useful reliability benchmark value.In cases where the measured threshold change was under 20% at a given temperature, τ_{laser} was obtained by linearly extrapolating to the estimated time for a 20% increase.The vertical bars in fig.4.2.0 include the range of τ_{laser} values, and the circles are average values for all devices tested at a given temperature.The solid line is the best linear fit to the average values.It falls along a curve

$\tau_{laser}\alpha$ (E/kT), with E=0.95±0.2 eV.The dotted line, an extrapolation to temperatures lower than those used in the test, projects to an average time of about 10^6 hrs to reach 20% increase in the pulsed laser threshold at 22°C.In practice, the cw threshold increase with time may be larger than the pulsed value if the thermal resistance of the laser increases.

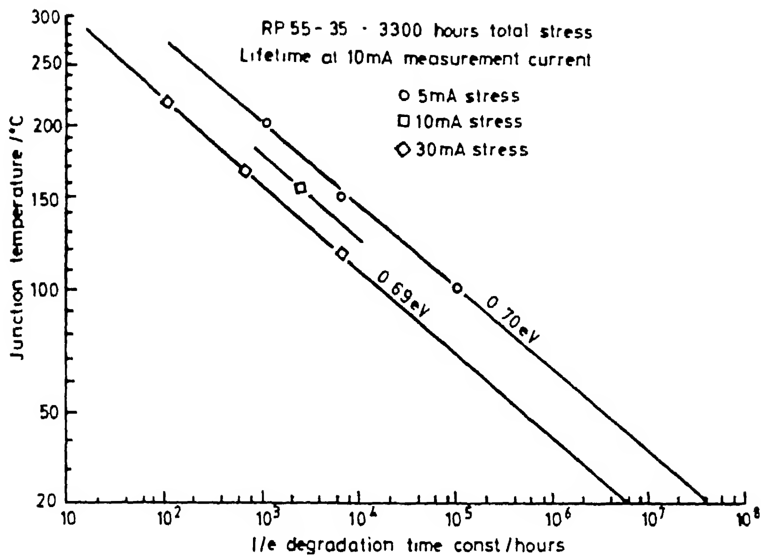

Fig.4·1·0 Arrhenius plot for red GaP LEDs aged at elevated temperatures and several values of drive current[113]

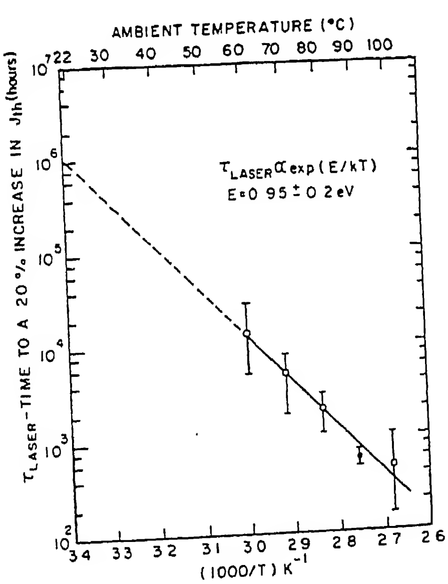

FIG 4.2.0 Time, at various ambience temperatures, needed to reach a 20% pulsed threshold current increase. The circles are the average values determined from the devices operated at a given temperature, whereas the bar give the range of values. The solid line is a linear "best fit" to the average values; the dotted line is an extrapolation to lower temperatures.

CHAPTER 5

REVIEW OF FIBER OPTIC TEMPERATURE SENSORS AND THEIR MARKET AREAS

5.01. INTRODUCTION:

Recently many types of temperature sensors using optical fiber either as the transduction eliment or as a communication link to an optical sensor, have been developed. Table-3 (repeated here for convenience) summarises various temperature sensors which uses fiber as a means of communication to and from the sensing eliment. A brief description of each of these sensors is presented here.

5.02. USE OF WAVELENGTH DEPENDENT EFFECTS: [19]

The use of wavelength dependent effects, with resulting colour changes, has been an attractive scheme for temperature sensing as referencing to the absolute light intensity is not required, the information being encoded in the wavelength of the light emergent from the sensor. For example band edge shifts in semiconductors (eg. GaAs) or doped glasses which contain semiconductors have been exploited in sensors and early problems with LED wavelength drift may be overcome through the use of high power, infra-red LEDs operated well below their maximum power or inexpensive laser diodes.

5.03. USE OF TEMPERATURE DEPENDENCE OF TRANSMISSION: [20, 21, 22, 23].

There have been many proposals for systems which incorporate a referencing technique and an example is proposed using optical absorption technique where the characteristics of

the transmission of the material changes with its temperature.Here the temperature dependent shift in the absorption edge of a small sample of GaAs is sensed using two widely seperated wavelengths of 0.88μm and 1.3μm.The shorter wavelength is attenuated by the change in absorption of the semiconductor with temperature while the longer wavelength is transmitted through the sample,unaffected by the temperature.

Some authors developed a system to utilise the change in absorption of ruby glass probed in the visible region of the spectrum by light from a dye laser at 605 and 622nm.Although these later two schemes use wavelength of close proximity to minimise differential transmission errors,maximum range of the device is limited due to the absorption edge affecting the longer wavelength transmission and restricting the wavelength range over which referencing is available.

5.04. USE OF TEMPERATURE DEPENDENT FLUORESCENT DECAY TIME: [24,25].

Another group of sensors addressed by multimode fiber optics, depend on the fluorescent decay time of the sample to a chopped light pulse for a measure of the temperature.The major advantage of this technique, monitoring the change "decay time" as a measure of temperature is that it obviates the need to make an accurate measure of the input light intensity but simply depends on measuring the time between two reference points on the fluorescence decay as shown below.

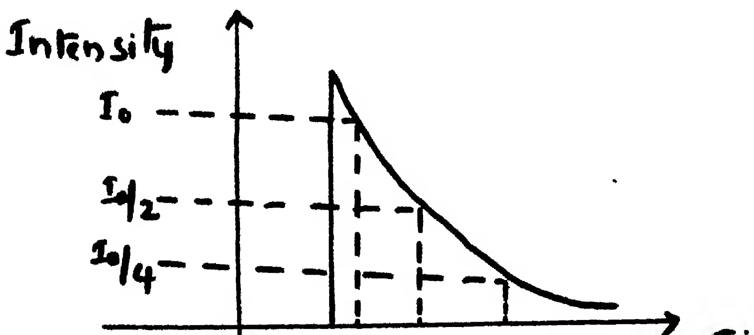

$$I = I_o \exp(-t/\tau)$$

Measurement made as,

$$I \longrightarrow \frac{I_o}{2} \ (t_2 - t_o) \text{ or}$$

$$I \longrightarrow \frac{I_o}{4} \ (t_4 - t_o)$$

The intensity of radiation emitted I(t) at a time "t" after the termination of the exiting pulse is given by

$$I = I_o \exp(-t/\tau)$$

where "τ " is the temperature dependent decay time.The time characterising the temperature dependent decay is measured as the time interval between the intensity I_o and a constant fraction of I_o.

The decay time of fluorescence concept using uv lamp excitation of phosphors such as ZnCdS and ZnSe was described in principle illustrating a biological range bulk optical sensor (40°C) using fluorescence decay in ruby.Another group produced a fiber optic sensor based on the decay time change in $BaClF:Sm^{+2}$ which operated up to ~150°C also using a mechanically modulated conventional lamp source.More recent work used a chromium doped crystal excited in the red with decay time principle to sense temperatures in the range from room temperature to ~200°C.

Another group of workers summarised the properties of the materials Neodymium,Alexandrite for use in the fluorescence decay time temperature sensor.These materials were chosen for their well known stability and for the fact that they are compatible for light excitation with the available lasers and LEDs and the decaying fluorescence may be measured with available solid state

detectors.The authors pointed out that the decay times of these fluorescent emitters is of the order of hundreds of microseconds and thus capable of being measured accurately by available electronic means,reference to megahertz quartz oscillators.Additionally these fluorescent materials have been used as the generators of a second reference wavelength at the sensor head itself,through the conversion of a small fixed fraction of the input light to longer wavelength fluorescence.

5.05. USE OF FIBER ITSELF AS THE SENSOR ELEMENT:[26].

A range of true intrinsic sensors using the fiber itself as the sensor element has been described;using either ordinary silica fiber or specially produced fiber.In the former case using optical time domain reflectometry (OTDR) the use of nonlinear interactions results in a temperature measurement being made from Raman scatter data.OTDR is a system which uses the time resolved information on the propagation of a short pulse in a fiber to determine positional information over a fiber length.The Raman effect is a nonlinear scattering effect in which a modulation of the light by interaction with the molecules of fiber material occurs.The wavelength of light is shifted to a longer wavelength (the so called Stokes line) and a shorter wavelength (the AntiStokes line) in addtion to scattering at the input wavelength (Raleigh scattering).A high power optical pulse is used to enable adequate levels of detection of the smaller scatter fraction to be made.The ratio of the AntiStokes to Stokes intensity is a function of the absolute temperature of the fiber and the signal received.Measurements with temperature resolution of 5K and spatial resolution of ~5m have been reported.

Special doped fibers are more expensive to manufacture than regular communication-type silica fiber but using Eu^{3+} and Nd^{3+} doped fibers it is possible to describe a sensor which relies upon the differential spectral absorption characteristics of the material.In the latter case,in Nd^{3+},an absorption band centered at ~800nm decreases in intensity while there is a corresponding increase in a band centered at ~860nm.The ratio is measured as a temperature dependent function.Recent results have shown that measurements up to~900°C can be made using Nd^{3+} and other rare earth doped fibers.

5.0.6. USE OF INDIRECT BANDGAP SEMICONDUCTORS: [27]

A temperature sensor based on the absorption properties of an indirect semiconductor has potentially superior properties to one based on a direct semiconductor such as GaAs and CdTe.Preliminary results are reported on a simple pointwise,single ended fiber optic sensor utilising a 10μm layer of single crystal silicon as the temperature sensitive material.Measurements in the range 20-180°C indicate that with a single wavelength (GaAs centered at 950nm) the discrimination of the device is ±0.2°C with an accuracy of about 4°C.Errors are believed to arise from thermal strains in the sensor head materials.With an antireflection coating on the Si layer a discrimination of ±0.12°C was achieved.

5.0.7. USE OF FIBER OPTIC TEMPERATURE SENSORS IN TRANSFORMERS: [28]

Fiber Optic temperature sensors were embedded directly with in the windings of a large transformer to measure "hot spot" temperatures under a variety of loading conditions.Sensor readings correlated well with the results from other measuring

devices in locations where a direct comparision could be made.It was demonstrated that accurate conductor temperature data can be obtained,but the probe insertion methods are critical.The data obtained have been useful in factory performance testing, in checking thermal modelling assumptions and calculations,and in estimating presently an un used transformer capacity.

5.0.8. USE OF CHANGE OF PHASE OR POLARISATION: [29,30].

Sensors based on the change of phase or polarisation of light can be configured as fiber optic interferometers and the interaction of a measurand, such as temperature with one arm of the device will result in a phase difference,for example between the modulated light in the measuring arm and light in a reference arm which is unaffected by the measurand.The optical signals from the two arms may be combined in,for example,the Mach-Zehnder fiber interferometer,to produce an interference pattern due to this phase difference which will vary with a change in the influence of the measurand on that arm of the device.

5.0.9. USE OF GaAsP CHIPS RETRIEVED FROM LEDs: [31].

GaAsP chips retrieved from ordinary red LEDs can be used as inexpensive,reproducible and durable temperature sensors over the range 4-300K.The variation with temperature of the forward voltage of the LED is exploited here.The low thermal mass results in response time below 25K, of considerably less than 1ms.

5.10. OPTICAL FIBER SENSOR MARKETS: [32,33]

A qualitative market summary of fiber optic sensors by application sector is shown in Table-A.Five main market areas have been defined as :military,manufacturing industries,consumer,and medical and chemical instrumentation.

Depending on the market importance, the sensors are classified as large,medium,and small markets which are estimated to have.They are shown in Tables-1,2,3 respectively.

A review of optical fiber sensor markets shows an extremely wide diversity of sensor types and a multitude of different applications.In many of these apllications fiber optic sensors carry real technical advantages and correspond to real market needs.Further research and development should improve their characteristics and usability and provide a firm commercial basis for a steady market growth.

TABLE-2

FIBER OPTIC TEMPERATURE SENSORS

Basic principle	Temperature range	Material used	Ref.
Temperature dependence of fluorescence decay time.	20-150°C (±1°C)	Crystal alexandrite	[24]
	15-130°C (±1°C)	Nd:glass	[25]
	35-46°C (±.3°C)	Pink ruby $Cr^{3+}:Al_2O_3$	[34]
	30-200°C (±5°C)	$BaClF:Sm^{2+}$	[35]
Temperature dependence absorption change in semiconductors/ other materials	-55-125°C (.1°C)	Ga As	[20]
	-60-200°C (±.5°C)	Nd:glass	[21]
	25-300°C (±10%)	Nd^{3+} doped glass	[22]
	-10-300°C (±1°C)	GaAs/CdTe	[23]
	20-180°C (±.2°C)	GaAs/CdTe	[36]
	25-45°C (±.05°C)	Thermochromic solution	[37]
	20-180°C (±.2°C)	Silicon	[27]

TABLE-2 CONTD...

Basic principle	Temperature range	Material used	Ref.
same as above	77-150K ($\pm$.5K)	Eu^{3+} doped fluoride glass	[38]
Raman back scattering	-30-67°C	----	[26]
Change in λ distribution of fluorescence	25-160°C ($\pm$.3°C)	Pink ruby $Cr^{3+}:Al_2O_3$	[19]
Change of polarisation with temper-ature	25-180°C	Quartz crystal	[29]
Change of no.of fringes with temperature	20-140°C	Fiber	[30]

BLE A - OPTICAL FIBRE SENSOR MARKETS BY APPLICATION SECTOR

	APPLICATION	Research effort	Advantages/ driving forces	Market importance	Development time
	- Fibre gyro	xxx	xxx	xxx	xxx
	- Under-sea detection (hydrophones, magnetometers)	xxx	xxx	xx	xx
	- Aircraft flight controls	xx	xx	xx	xxx
	- Aircraft engine monitoring	xx	xx	xx	x
	- Nuclear radiation testing	xxx	xxx	x	x
	- Chemical analysis	xx	xxx	xxx	xx
	- Security systems	xx	xx	xxx	xx
INDUSTRIES	- Automation	x	x	xx	xx
	- Machine tool control	x	xx	xx	xx
	- Inspection/Metrology	xx	xx	xxx	x
	- Robotics	x	x	x	xx
	- Process control	xx	xx	xxx	xxx
	- Chemical instrumentation	xx	xxx	xxx	xx
INDUSTRY	- Geophysical prospection	xx	xx	xxx	xx
	- Petrochemical plants	xx	xxx	xx	xx
	- Mining	x	x	xx	xxx
	- Electricity supply (transmission/ plant control)	xxx	xx	xx	xxx
	- Gas/water utilities (wastewater treatment	x	x	x	xx
CONSUMER	- Automobile	xx	x	xxx	xx
	- Electrical appliances	x	x	xx	xxx
	- Building Management Systems (comfort and energy control, fire and intrusion security)	x	xx	xx	x
	- Data processing equipment (office equipment, POS)	x	xx	xxx	x
MEDICAL AND CHEMICAL	- Diagnostic equipment	x	xx	xx	xx
	- Surgical support (oximetry, blood flow)	xx	xx	xx	xx
	- Spectrometers (colourimeters, pH)	xx	xxx	xxx	x
	- Pollution monitoring	x	xx	xx	xx

ey		xxx	xx	x
	Research effort:	large (5 M $)	Moderate	Small (0.5 M $)
	Advantages:	major	some	minor
	Market Importance:	large	medium	small
	Development time:	long (10 years)	medium	short (1-3 years)

The following are estimated to have large markets, of the order of thousands:

Carbon dioxide, blood (FO)	Medical diagnosis
Colorimeter (low cost)	Medical diagnosis
Gas sensors (breath analysis)	Medical diagnosis
Ion selective FETs	Medical diagnosis
Ion selective electrodes (thin film)	Medical diagnosis
Oxygen, blood (FO)	Medical diagnosis
Pressure (FO)	Aeronautical, cars

Table 1

The following are estimated to have medium markets, of the order of hundreds:

Accelerometer (FO)	Helicopter gearbox
Antigens (immunospecific)	Cancer research
Biomass (non invasive)	Pharmaceutical
Bubble size, number	Pharmaceutical
Calcium ions (optical sensor)	Pharmaceutical
Carbon dioxide	Coal
Carbon dioxide (bioreactors)	Pharmaceutical
Carbon monoxide	Environmental
Current (high voltage lines, FO)	Railways
Cyanide ion (rivers)	Water pollution
Displacement (high voltage wires)	Railways
Displacement (radiation resistant)	Nuclear power
Displacement (remote)	Pharmaceutical
Displacement (turbine blade)	Jet engine design
Dust in air (radiation resistant)	Nuclear power
Freon-22 (breath)	Medical diagnosis
Fuel level (FO)	Aeronautical
Gamma ray (micro)	Cancer research
Gas velocity (flow measurement)	Jet engine design
Heavy metals	Water pollution
Hydrogen	Coal
Hydrogen (trace, breath)	Medical diagnosis
Hydrogen sulphide	Environmental
Light scattering (sterile liquids)	Pharmaceutical
Liquid level (radiation resistant)	Nuclear power
Magnesium ions (optical sensor)	Pharmaceutical
Mass (radiation resistant)	Nuclear power
Mass (remote)	Pharmaceutical
Methane (traces)	Gas
Nitrate ion (rivers)	Water pollution
Nitric oxide (dissolved, ppb)	Pharmaceutical
Nitrogen oxides	Environmental
Oxygen	Coal
Oxygen (bioreactors)	Pharmaceutical
PH (bioreactor)	Pharmaceutical
PH (remote, radiation resistant)	Nuclear power
Pressure (radiation resistant)	Nuclear power
Pressure (remote)	Pharmaceutical
Strain (FO)	Helicopter blades
Temperature (micro)	Cancer research
Temperature (radiometric)	Jet engine design
Temperature (remote)	Pharmaceutical
Tension	Railway lines
Torque (bioreactor agitator)	Pharmaceutical

Table 2

The following are estimated to have small markets, of the order of tens:

Calorimeter (diff scanning, micro)	Pharmaceutical
Gamma ray (micro)	Pharmaceutical
Ground velocity (optical)	Railways
Heat output (organs)	Cancer research
Ionic strength (remote)	Nuclear power
Light output (luminescent displays)	Aeronautical
Neptunium (IV, remote)	Nuclear power
Nitrate ion (remote)	Nuclear power
Plutonium (III, IV, remote)	Nuclear power
Raman microspectroscopy	Pharmaceutical
Solvent vapours (work area)	Pharmaceutical
Spectral emission, plasma	Semiconductor dev.
Strain (circumferential, FO)	Jet engine design
Strain (micro sensor)	Pharmaceutical
Strain (tablet dies)	Pharmaceutical
Temperature (distributed)	Cancer research
Temperature (high voltage lines)	Railways
Temperature (micro, leadless)	Pharmaceutical
Temperature (radiometric)	Pharmaceutical
Thermal imaging (crack detection)	Nuclear power
Torque (high temperature)	Jet engine design
Uranium (IV, VI, remote)	Nuclear power

Table 3

CHAPTER 6

CONCLUSIONS

In this work the results which have been obtained to explore the possibility of using light emitting devices as fiber optic temperature sensors are reported.Electroluminescent spectra of each of the LEDs was measured and the peak wavelength of emission was noted which helps to identify the material from which the LED was fabricated.Commercially available LEDs which emit in the green and red parts of the visible spectrum were considered.Temperature dependence of the degradation of the output power of the device was used to characterise a particular device in order to use it as a temperature sensor.

Temperature aging tests at a fixed driving current were carried out.It was observed that the degradation of GaP:N LEDs with temperature was less, of about 1.6 dBm over a temperature range of 25-120°C.Moreover the degradation observed was not uniform, which is a drawback for the calibration of the device.With these two things in mind, we can as well say that GaP:N LEDs do not appear to be suitable as temperature sensors.

Similar tests of temperature stress-aging were carried out for red LEDs made from GaP:N,$Ga_{0.6}As_{0.4}P$,$Ga_{0.7}Al_{0.3}As$ at a constant current.Among these three types, large power output change of about 6 dBm was obsreved in GaP:Zn,O LEDs over a temperature range of 30-140°C.In addition the degradation is almost uniform, which is an advantage when calibrating the device for temperature measurement.On the other hand the degradation in the case of $Ga_{0.7}Al_{0.3}As$ LEDs is minimum over the same

temperature range.And the power output versus temperature curve was more or less linear.Finally the power output variation of GaAsP LEDs with temperature was in between those of GaP:Zn.O and GaAlAs with the similar uniform degradation.

From the experimental results presented in chapter-3, it appears that use of GaP:Zn,O LEDs as temperature sensors is feasible as they exhibit large output power change over the temperature range of interest.Even the other two types of red LEDs are also suitable, as the difference in the observed characteristics was not much.If we can eliminate some of the technical problems like coupling of light output power in the fiber,detection of emission, then we can use any or all of the red LEDs mentioned in this study.Suggestions were made to increase the coupling of power by using the compatible connectors so as to obtain good resolution.

In semiconductor lasers the threshold current dependence on the temperature can be exploited to design fiber optic temperature sensors.As an attempt, schemes were suggested for the measurement of threshold current using optical methods.A purely eléctrical measurement technique for the measurement of threshold current was described with experimental setup.The threshold current measured in this way can be used to compare the result obtained from the conventional ways.The low reliability of semiconductor lasers is a major disadvantage for use as temperature sensors.Because in the process of temperature stressing many of them may get damaged.Better fabrication techniques, which results in reliable components, may permit us to use semiconductor lasers for designing temperature sensors.

Optoisolators can be used as temperature sensors over a range of 0-85°C.The advantage here is that the coupling of power is done internally from the source to the detector.The degradation of current transfer ratio (CTR) with temperature can be exploited for use as temperature sensors.The disadvantage is that, these optrons can not be operated at higher temperatures, in which case the coupling of power from the source to the detector becomes less.

REFERENCES

[1].Giallorenzi,T.G. et.al "Optical fiber sensor technology" IEEE J. Quantum Elect.,**QE-18**,626,(1982).

And G.D.Pitt et.al "Optical fiber sensors" IEE Proc-J Optoelectronics,**132J**,214 (1983).

[2].First international conference on "Optical fiber sensors" organised by IEE, p-55,(1983).

[3].O.N.Ermakov et.al "Temperature behaviour of bright luminescence from LPE-grown $Ga_{1-x}Al_xP$ structures" IEEE Trans.Elect.Dev.**ED-30**,268,(1983).

[4].Optoelectronics/Fiber opt: s Application manual (Hewlett Packard),McGrahill book company, p-1.8 (1981)

[5].H.Albrecht "The role of nitrogen on the degradation behaviour in LPE and VPE GaP:N LEDs" IEEE Trans.Elect.Dev **ED-30**,259, (1983).

[6].P.M.Petroff et.al "Defect structure induced during the forward bias degradation of GaP green LEDs" J.Appl.Phys.**47**, 1583 (1976).

[7].K.Kaneko, "Degradation of GaP green LEDs" Japan.J.Appl.Phys. **15**,1287,(1976).

[8].J.M.Ralston et.al "Degradation of bulk electroluminescent efficiency in Zn,O-doped GaP LEDs" IEEE Trans.Elect.Dev.**ED-24** 970,(1977).

[9].H.Schade et.al "Direct evidence for generation of defect centres during forward bias degradation of $GaAs_{1-x}P_x$ electroluminescent diodes" J.Appl.Phys. **42**, 5072 (1971).

[10].J.M.Ralston et.al "Temperature and current dependence of red emitting GaP LEDs" J.Appl.Phys. **50**,3630,(1979)

[11].M.Asada et.al "The effects of loss and nonradiative recombination on the temperature dependence of threshold current in 1.5-1.6μm GaInAsP/InP lasers" IEEE J.Quant.Elect. **QE-19**, 917,(1983).

[12].L.Sharupich,N.Tugov "Optoelectronics" Mir Publishers,**Chap-3** (1984).

[13].E.W.Williams & R.Hall "Luminescence and the light emitting diode", Pergamon press,p105,(1978)

[14].H.Kressel, Topics in applied physics V.39 "Semiconductor devices for optical communications" Spriger verlag,**Chap-8** (1982).

[15].T.L.Paoli et.al "Derivative measurements of the current-voltage characteristics of double-heterostructure injection lasers" IEEE J.Quant.Elect. **QE-12**,633,(1976).

[16].J.M.Ralston et.al "Temperature and current dependence of degradation of red emitting GaP LEDs" J.Appl.Phys.**50**, 3630 (1979).

[17].Howes and Morgan "Reliability and Degradation" John Wiley &sons **Chap-6** (1980).

[18].H.Kressel et.al "Accelerated step-temperature aging of $Al_xGa_{1-x}As$ heterojunction laser diodes" Appl.Phys.Lett.**32**, 305,(1978).

[19].KTV.Grattan et.al "Fiber optic temperature sensor using change in the wavelength distribution of emission of fluorescence" Rev.Sci.Inst.**56**,1231 (1987).

[20].M.M.Sallour et.al "Semiconductor platelet fiber optic temperature sensor" Electron.Lett.**21**,135,(1984)

[21].KTV.Grattan et.al "Fiber optic temperature sensor using fluorescence reference channel" Rev.Sci.Inst.**57**,1175,(1986).

[22].G.Adamovsky et.al "Fiber optic thermometer using temperature dependent absorption,broadband detection and time domain referencing" Appl.Opt.**25**,4439,(1986).

[23].Kyuma et.al "Fiber optic instrument for the measurement of temperature" IEEE J.Quant.Elect.**QE-18**,676,(1982).

[24].A.T.Augoustiet.al "Visible LED pumped fiber optic temperature sensor" IEEE Trans.Instr.&Meas.**37**,470,(1988).

[25].KTV.Grattan et.al "Infrared fluorescence decaytime temperature sensor" Rev.Sci.Inst.**56**,1784,(1985).

[26].J.K.A.Everard et.al "Distributed optical fiber Raman temperature sensor" Electron.Lett.**21**,569,(1985).

[27].I.Kajanto et.al "A silicon based fiber optic temperature sensor" J.Phys.E:Sci.Instr.**21**,652,(1988).

[28].K.A.Wickersheim et.al "Improved fiber optic temperature measurement system for monitoring winding temperatures in medium and large transformers" IEEE Trans.Power Delivery, **PWRD-2**,831,(1987).

[29].A.J.Rogers "Optical fiber temperature sensor for high voltage applications" Appl.Opt.**21**,882,(1982).

[30].S.S.Gattani "Interferometric fiber optic temperature sensor" M.Tech Thesis (EE),IIT/Kanour,FEB-1990.

[31].B.F.Griffing et.al "Use of light emitting diodes as temperature sensors" Rev.Sci.Inst.**48**,1225,(1977).

[32].First international conference on "Optical fiber sensors" organised by IEE,p56,(1983).

[33].B.J.Meggitt et.al "Optical and semiconductor sensors in

laboratory and scientific instrumentation"Meas.+control **22**,37,(1989).

[34].R.R.Sholes et.al "Fluorescent decay thermometer with biological applications" Rev.Sci.Inst.**51**,881,(1980).

[35].J.S.McCormak et.al "Luminescent decay temperature sensor" Electron.Lett.**17**,630,(1981).

[36].I.Kajanto et.al "Fiber optic temperature sensor" J.Phys.E: Sci.Inst.**21**,652,(1988).

[37].Maurobacci et.al "Thermochromic optical fiber temperature sensors" Appl.Opt.**25**,1079,(1986).

[38].Ohishi et.al "Fiber optic rare earth temperature sensor" Appl.Opt.**25**,720,(1986).